Icarus 316 (2018) 167–190

Contents lists available at ScienceDirect

Icarus

journal homepage: www.elsevier.com/locate/icarus

Geologic mapping of the Urvara and Yalode Quadrangles of Ceres

David A. Crown[a,*], Hanna G. Sizemore[a], R. Aileen Yingst[a], Scott C. Mest[a], Thomas Platz[a,b], Daniel C. Berman[a], Nico Schmedemann[c], Debra L. Buczkowski[d], David A. Williams[e], Thomas Roatsch[f], Frank Preusker[f], Carol A. Raymond[g], Christopher T. Russell[h]

[a] Planetary Science Institute, 1700 E. Ft. Lowell Rd, Suite 106, Tucson, AZ 85719 USA
[b] Max Planck Institute for Solar System Research, Gottingen, Germany
[c] Freie Universitat Berlin, Berlin, Germany
[d] Planetary Exploration Group, Johns Hopkins University Applied Physics Laboratory, Laurel, MD 20723 USA
[e] School of Earth and Space Exploration, Arizona State University, Tempe, AZ 85287 USA
[f] German Aerospace Center, DLR, Berlin, Germany
[g] NASA Jet Propulsion Laboratory, Pasadena, CA 91109 USA
[h] Institute of Geophysics and Planetary Physics, University of California at Los Angeles, Los Angeles, CA 90024 USA

ARTICLE INFO

Article history:
Received 30 November 2016
Revised 21 July 2017
Accepted 1 August 2017
Available online 5 August 2017

ABSTRACT

We conducted geologic mapping of the Urvara (Ac-13) and Yalode (Ac-14) Quadrangles (21–66°S, 180–360°E) of the dwarf planet Ceres utilizing morphologic, topographic, and compositional information acquired by NASA's Dawn mission. The geologic characteristics of the two large impact basins Urvara (170 km diameter) and Yalode (260 km diameter) and their surroundings were investigated using Dawn Framing Camera datasets, including Survey (415 m/pixel), HAMO (140 m/pixel), and LAMO (35 m/pixel) images and mosaics, color and color ratio images, and DTMs derived from stereo-photogrammetry. Geologic mapping demonstrates that impact cratering has dominated the geologic history of the Urvara and Yalode Quadrangles, with early cratered terrain formation followed by formation of the large basins and widespread emplacement of basin-related smooth material. Impact craters display a wide range of preservation states from nearly completely buried/degraded forms to more recent pristine craters with terraced inner walls and lobate ejecta deposits. Cross-cutting relationships and morphologic signatures show that the Urvara impact followed the Yalode impact, consistent with ages derived from crater size-frequency distributions (580 ± 40 Ma for Yalode and 550 ± 50 Ma for Urvara). Observed differences in basin materials and rim morphology suggest heterogeneities in the substrate excavated by impact. Smooth deposits that cover large areas of the quadrangles, including the basin floors, rims, and exterior zones, are interpreted to be dominated by Urvara ejecta but Yalode ejecta and localized ice-rich flow material may be minor components. Geologic mapping results and simulations of ejecta emplacement suggest that Urvara and Yalode ejecta deposits extend for large distances (more than two crater diameters from the basin centers) and may serve as important stratigraphic markers for the geologic record of Ceres.

1. Introduction

NASA's Dawn spacecraft, launched in September of 2007, orbited the asteroid Vesta in 2011 and 2012 and was inserted into orbit around Ceres on March 6, 2015, where it continues to return imaging, spectroscopic, and elemental datasets from the dwarf planet (e.g., Russell and Raymond, 2011; Russell et al., 2016). Central to the Dawn Mission is characterization of early Solar System conditions through geologic analyses of and comparisons between the small, differentiated, rocky protoplanet Vesta and larger Ceres (1/3 of the mass of the asteroid belt), whose spectral characteristics had suggested a water-rich, carbonaceous chrondrite-like composition (e.g., McCord and Sotin, 2005). This study reports on detailed geologic mapping of two 1:500,000-scale quadrangles (Ac-13 and Ac-14) in Ceres' southern hemisphere covering the region 21–66°S, 180–360°E and containing the large impact basins Urvara and Yalode (Fig. 1). We present a map-based description of the geology, a synthesis of the geologic history of the region of interest, and analyses of impact basin morphology on Ceres. We also

* Corresponding author.
E-mail address: crown@psi.edu (D.A. Crown).

http://dx.doi.org/10.1016/j.icarus.2017.08.004

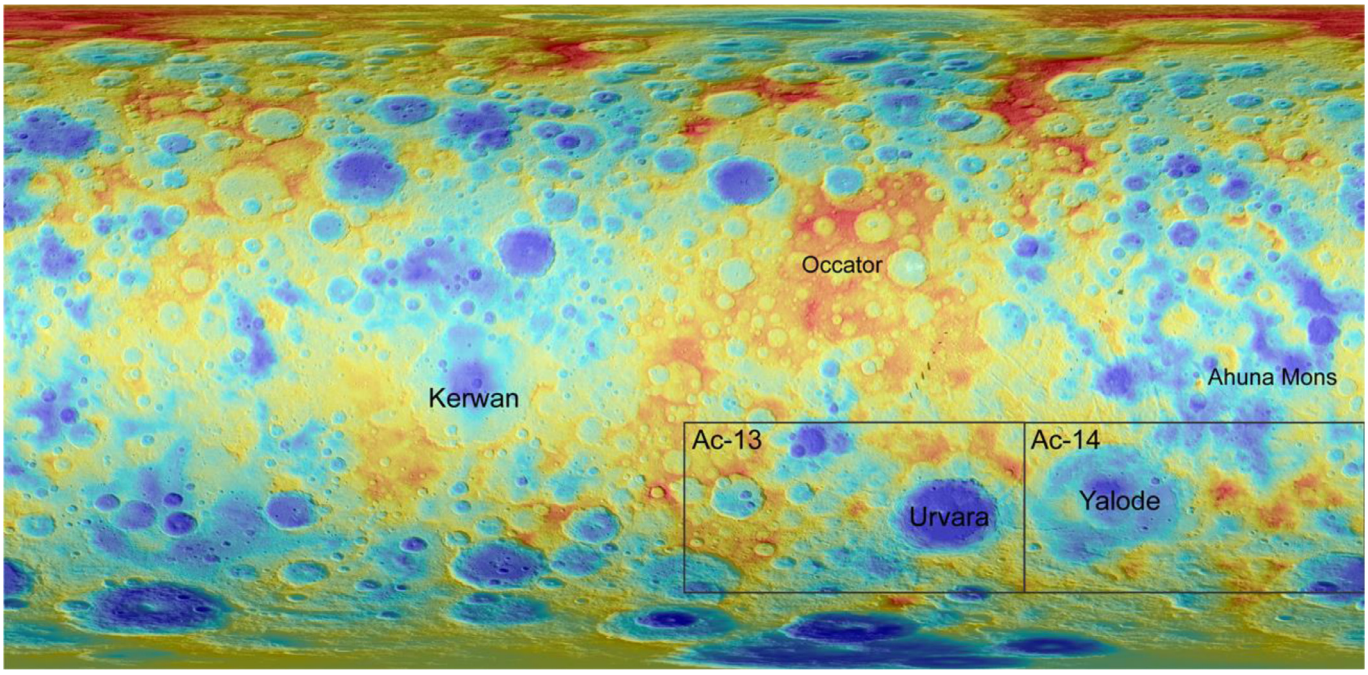

Fig. 1. Global 60 pixel/degree (137 m/pxl) Digital Terrain Model (DTM) (Preusker et al., 2016) over HAMO image mosaic (Roatsch et al., 2016) showing the locations of the Urvara (Ac-13; 21–66°S, 180–270°E; left box) and Yalode (Ac-14; 21–66°S, 270–360°E; right box) Quadrangles of Ceres. DTM range in elevation is −7049 to 7499 m. Simple cylindrical projection with center longitude of 180°E. (For interpretation of the references to color in this figure legend, the reader is referred to the web version of this article.)

explore the implications of using these large impact basins on Ceres as stratigraphic markers.

2. Background

A key objective for the exploration of the dwarf planet Ceres by the Dawn Mission is to understand the role of water in the geologic history of a primitive body. Prior to the mission several lines of evidence suggested that Ceres was water-rich and its surface geology might have been strongly influenced by water and/or water ice. The relatively low density of Ceres indicates that it is a differentiated body with water concentrated in outer layers above a rocky core (Thomas et al., 2005; McCord and Sotin, 2005; Castillo-Rogez and McCord, 2010). Ceres' spectral characteristics have been attributed to silicate compositions along with carbonates and iron-rich clays (Rivkin et al., 2006), OH- or H_2O-bearing phases (Lebofsky et al., 1981, 1986; Rivkin et al., 2006), and aqueous alteration of olivine-rich materials (Milliken and Rivkin, 2009). Modeling studies showed the potential for recent or current hydrothermal activity (McCord and Sotin, 2005; Castillo-Rogez and McCord, 2010). In addition, observations from the Herschel Space Observatory showed localized water vapor emissions from Ceres that were interpreted to be due to sublimation of cometary ice exposed at the surface or cryovolcanism (Küppers et al., 2014).

Dawn observations of Ceres to-date have provided significant new insights into its geology and geologic history. Evidence for the presence, potential abundance, and/or effects of water ice include: a) measurement of variations in gravity confirming interior differentiation, with potential concentrations of water in outer, weaker layers (Park et al., 2016); b) mapping and modeling of cold traps in permanently shadowed areas in craters in the north polar region (Platz et al., 2016a; Schorghofer et al., 2016); c) imaging of the volcanic dome Ahuna Mons, whose morphology has been attributed to extrusive cryovolcanic activity (Ruesch et al., 2016); d) spectral detection of exposed water ice at Oxo Crater (Combe et al., 2016); e) spectral signatures of ammonium phyllosilicates, the presence of which suggests widespread alteration of the surface materials of Ceres (Ammannito et al., 2106); and f) deficits in thermal and epithermal neutron flux measured by the Gamma Ray and Neutron Dector (GRaND) consistent with the presence of subsurface ice at high latitude (Prettyman et al., 2016). In addition, bright spots associated with Occator and other craters on Ceres have been interpreted to indicate the presence of sodium carbonate and other salts that may result from hydrothermal activity (De Sanctis et al., 2016; see also Nathues et al., 2015, 2017). Analyses of Ceres' impact craters have revealed that 1) the current surface of Ceres is depleted in large craters (i.e., >100–150 km) relative to the expected population presumably due to impact-driven resurfacing (Hiesinger et al., 2016; Marchi et al., 2016), 2) polygonal forms and fractured floors reflect pre-existing structural patterns in fractured crustal materials (Buczkowski et al., 2016), and 3) morphologic attributes of some craters and the simple-complex crater transition diameter are consistent with impact into surface materials that are a mixture of ice and rock (Hiesinger et al., 2016).

The Dawn Science Team is leading a coordinated mapping program that will result in generation of (1) a global geologic map of Ceres (primarily based on HAMO (High Altitude Mapping Orbit) images (Mest et al., 2016; 2017)) and (2) 15 geologic maps of 1:500,000-scale quadrangles using LAMO (Low Altitude Mapping Orbit) images (Williams et al., 2017a and other papers in the current issue; see also Nass, 2017). Geologic mapping of Ceres has been undertaken to help integrate and synthesize observations made using Dawn Mission datasets in order to advance knowledge of Ceres' surface geology and geologic evolution, as well as to provide geologic and stratigraphic context for spectral and elemental data.

3. Dawn datasets

For geologic mapping of the Urvara and Yalode Quadrangles of Ceres, we utilized individual Framing Camera (FC) images and image mosaics, color and color ratio datasets, and digital terrain models (DTMs) derived from FC images (Preusker et al., 2016; Roatsch et al., 2016; 2017) (Fig. 2). Onboard the Dawn spacecraft there are

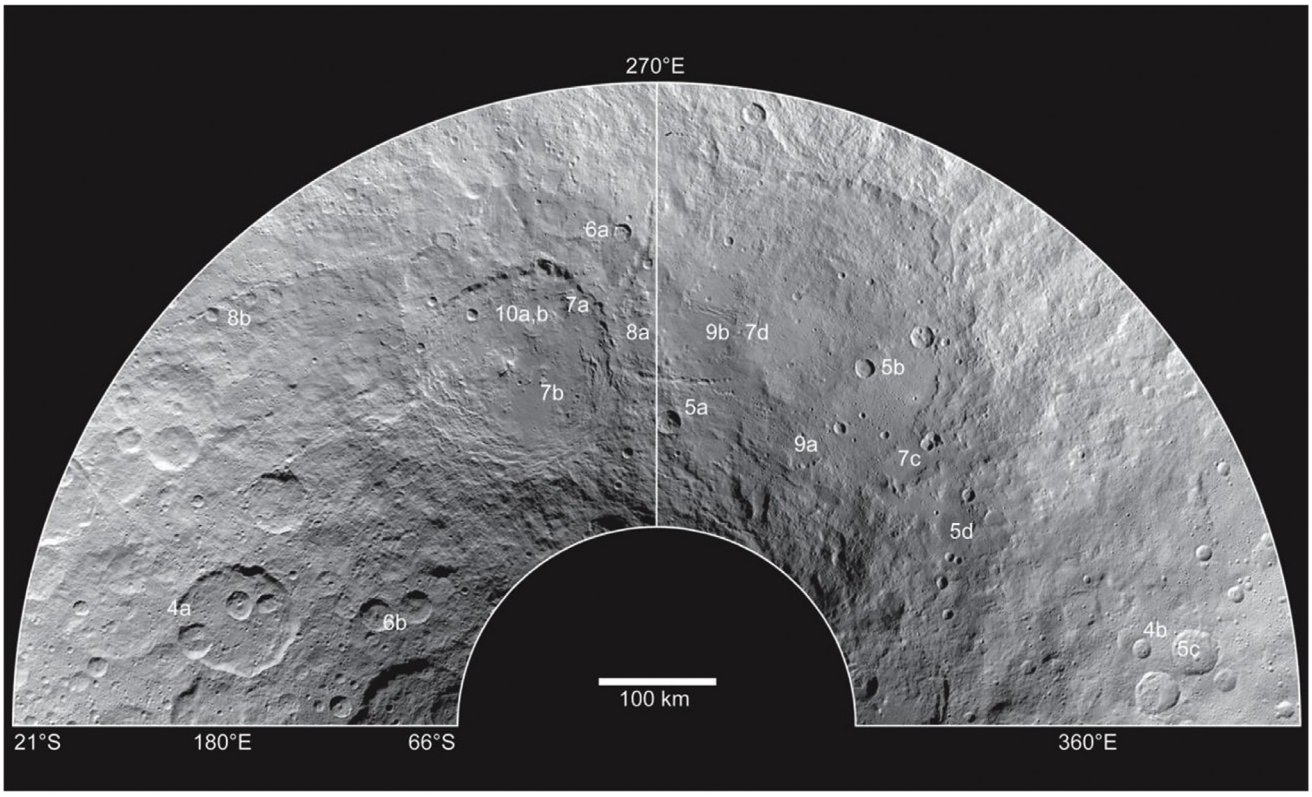

(a)

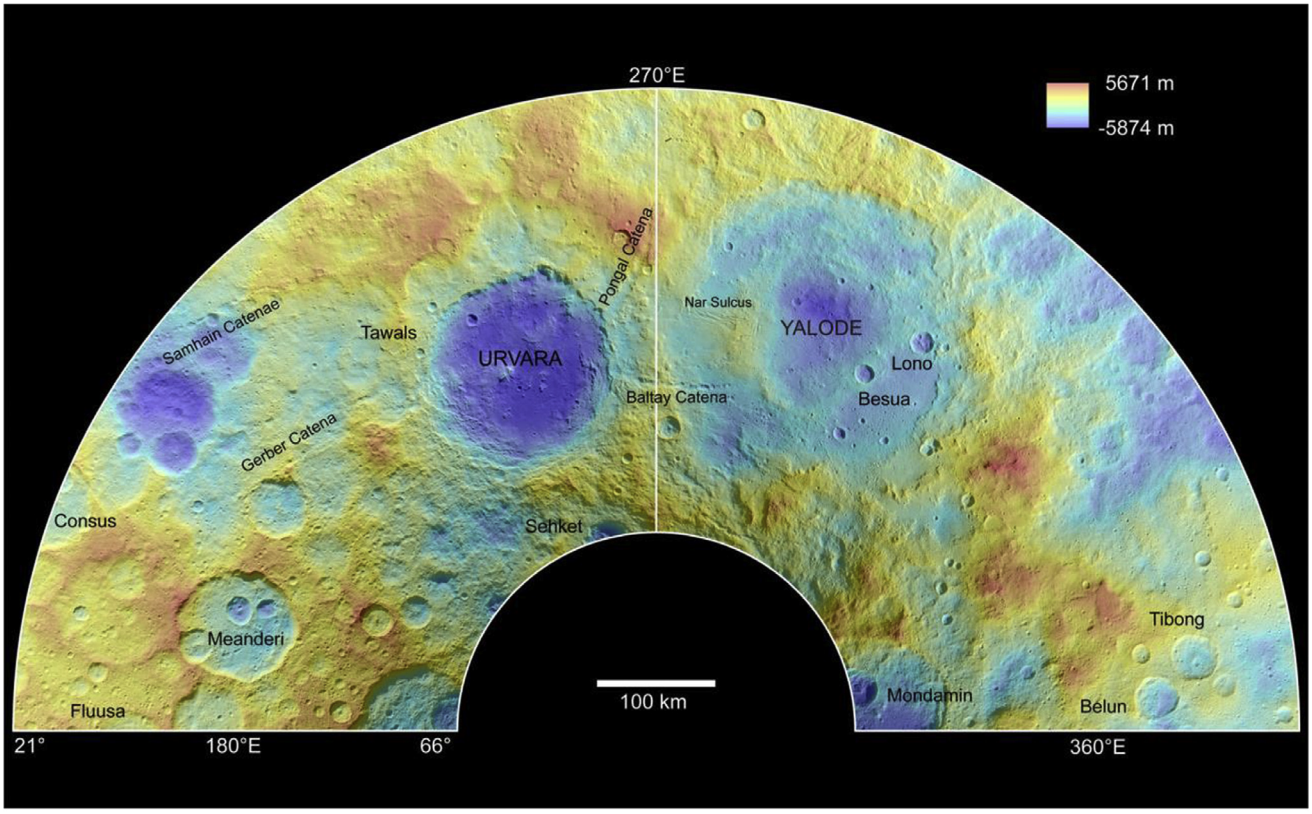

(b)

Fig. 2. Urvara (left) and Yalode (right) Quadrangles of Ceres: a) LAMO mosaic (35 m/pxl) with locations of Figs. 4–10 indicated, b) HAMO DTM (60 pixel/degree), c) HAMO photometrically-corrected, color mosaic (R = 965 nm, G = 750 nm, B = 440 nm; yellow shows area near south pole that is unusable due to high incidence angles), and d) Survey color composite image (using band ratios: R = 965/750 nm, G = 550/750 nm, and B = 440/750 nm). All images in Ceres polar stereographic projection centered on 270°E. Image mosaics (Roatsch et al., 2016, 2017), HAMO color, and DTM (Preusker et al., 2016) courtesy of DLR; Survey color composite courtesy of MPS.

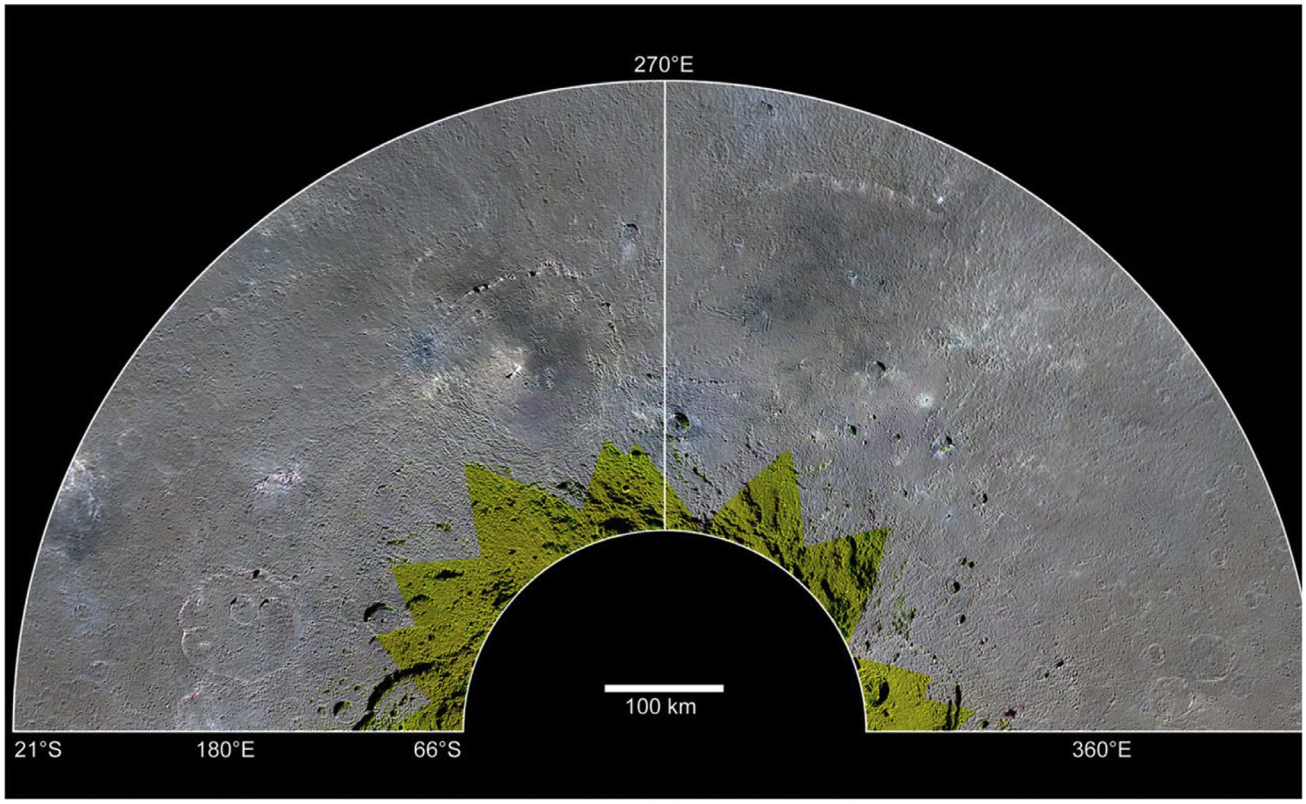

(c)

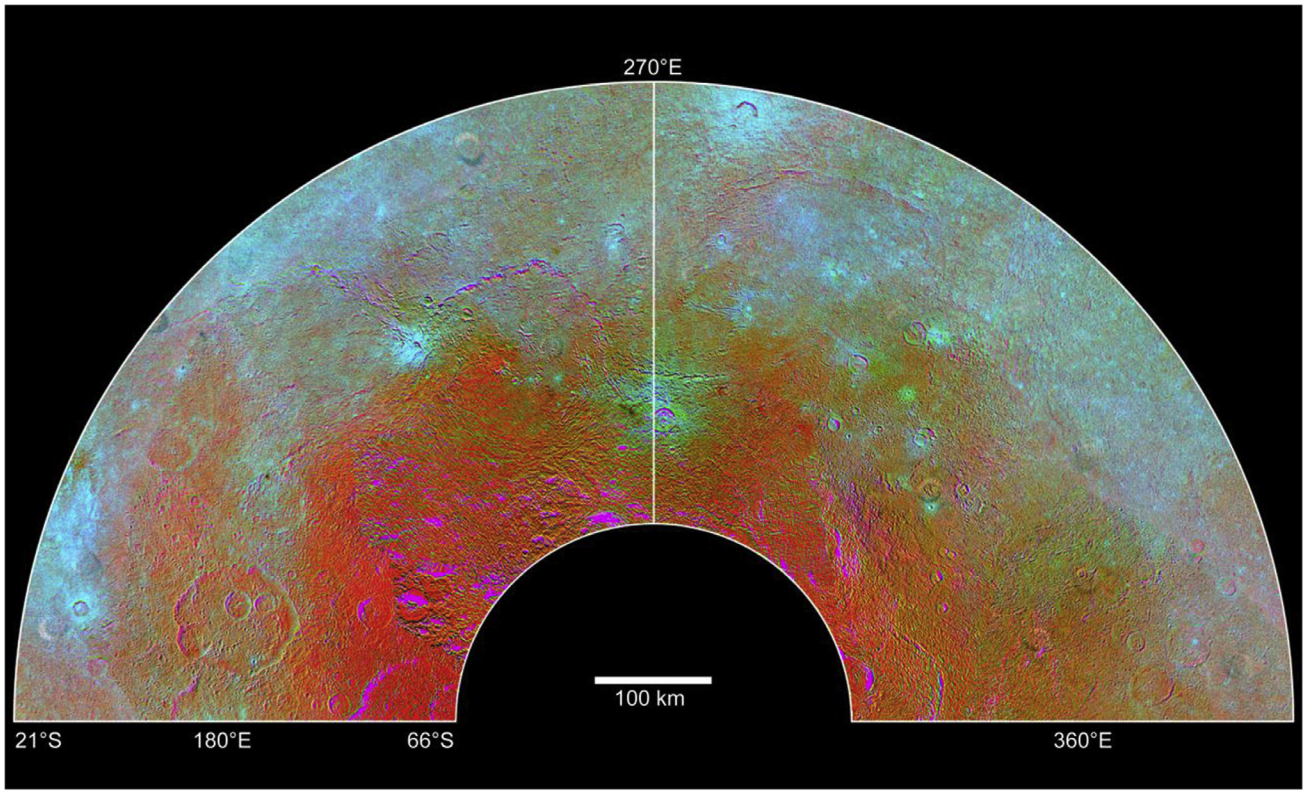

(d)

Fig. 2. Continued

two identical Framing Cameras (FCs) (Sierks et al., 2011); FC2 provided near 100% coverage of the surface of Ceres in clear filter mode (i.e., panchromatic; filter F1) during three planned orbital phases. Image resolution improved significantly through the Survey (415 m/pixel), HAMO (140 m/pixel), and LAMO (35 m/pixel; Fig. 2a) phases, and clear filter mosaics generated at each phase were used as bases for geologic mapping. We examined morphologic features, surface textures, and albedo in these mosaics.

The Dawn Framing Camera is equipped with eight filters (one clear and seven multispectral) covering a range of 420–980 nm, yielding global color data. FC data were radiometrically calibrated and photometrically corrected, stray light was removed, and data were converted to reflectance (I/F) (Nathues et al., 2014). The resulting reflectance data were map-projected and co-registered to generate color cubes, which were then mosaicked (Fig. 2c). A detailed description of the FC data processing pipeline is presented in Reddy et al. (2012). The result is a robust color mosaic that was used to refine unit boundaries and assist in interpreting unit stratigraphy. Color ratios (e.g., ratios similar to the "Clementine color ratio" utilized at Vesta (Reddy et al., 2012)) were also examined. To assist in and compare to geologic mapping, we used the following band ratio combination, as outlined in Reddy et al. (2012): R = 965/750, G = 550/750, B = 440/750 (Fig. 2d). In this ratio mosaic, the red channel is meant to highlight variations in the spectral signature at longer wavelengths, whereas green tones represent variations in the peak wavelengths often associated with albedo. The blue ratio provides an estimate of short wavelength variations, particularly the continuum slope; bluer tones may be approximately equated to less mature regolith. The color ratio mosaic was used with caution because it appears to be affected by shadow boundary issues and is thus difficult to interpret.

Dawn Framing Camera images have been used to derive digital terrain models (DTMs) for Ceres via stereo-photogrammetry (Preusker et al., 2016). Dawn acquired ~880 clear filter images during Survey orbit at ~415 m/pixel and ~2350 HAMO clear filter images at ~140 m/pixel. Images were acquired globally under similar illumination conditions but different viewing conditions to create a stereo constellation that was used to produce Survey and then HAMO (~140 m/pixel spatial resolution; 10 m vertical accuracy; Fig. 2b) DTMs. We utilized topographic information for landforms on Ceres to assist in unit identification and characterization and to assess contact relationships.

4. Geologic mapping of the Urvara and Yalode Quadrangles

Urvara and Yalode are adjacent impact basins located in the southern hemisphere of Ceres. These two impact basins dominate the geology of the 1:500,000-scale Urvara (Ac-13; 21–66°S, 180–270°E) and Yalode (Ac-14; 21–66°S, 270–360°E) Quadrangles (Fig. 1). Yalode is 260 km in diameter, centered at 42.3°S, 293.6°E; Urvara is 170 km in diameter, centered at 45.9°S, 249.2°E. They are the second- and third-largest distinct impact structures on Ceres after Kerwan (280 km diameter, 10.8°S, 123.6°E). To the east of Yalode is the subdued expression of a similar-sized circular depression, presumably the site of a degraded impact basin that predates Yalode. Urvara has a more well-preserved morphologic expression than Yalode, and structures radial to Urvara (including Baltay Catena) extend to the east across Yalode. Each basin is fully contained within the self-named quadrangle but distal impact deposits and structures extend into neighboring quadrangles, including the Zadeni Quadrangle to the south and the Occator and Rongo Quadrangles to the north. Urvara and Yalode basins occur within the cratered terrain that dominates much of the surface of Ceres. Ahuna Mons, an apparently unique volcanic extrusion on the surface of Ceres (Ruesch et al., 2016), is found in the Rongo Quadrangle to the northwest of Yalode basin.

We have produced geologic maps of the Urvara and Yalode Quadrangles using ArcGIS software and imaging and topographic data acquired by the Dawn spacecraft (see Section 3 and Williams et al., 2017a this issue). Base map image mosaics, DTMs, and color and color ratio datasets were used to identify, map the locations/distribution of, and describe geologic units and features. Geologic mapping layers included point features, geologic contacts, and linear features. Geologic contact polylines were converted into polygons to define geologic units. Survey and HAMO mosaics and a Survey-based DTM were used to define a preliminary set of geologic units for each of the quadrangles (Crown et al., 2015; Sizemore et al., 2015a, 2015b; Yingst et al., 2015). LAMO mosaics, the HAMO DTM, Survey color ratio data, and HAMO color data were used to refine and finalize the map unit scheme and to provide detailed unit characterizations (Fig. 2) (Crown et al., 2016a; 2016b; Sizemore et al., 2016a; 2016b; Yingst et al., 2016).

Fig. 2 shows the key datasets used for geologic mapping of Ceres. Both HAMO and LAMO (Fig. 2a) mosaics show smooth to rugged surfaces across the region encompassing the Urvara and Yalode Quadrangles. Smooth surfaces are prominent on the floors of the large basins and within basin rim zones, and also occur in the surrounding cratered terrain. The cratered terrain exhibits varied surface texture and morphology, controlled primarily by the abundance, size range, and degradation states of impact craters, which are observed to vary spatially across the region of interest.

The HAMO DTM (Fig. 2b) clearly shows well-defined depressions in the interiors of Urvara, Yalode, Meanderi (diameter = 103 km), and Mondamin (diameter = 126 km) as well as various small- to medium-sized craters scattered throughout the quadrangles. Locally high-standing, rugged terrain is evident surrounding these four impact structures and may represent parts of their continuous ejecta blankets. The cratered terrain exhibits significant variations in elevation across its surface and several discrete high-standing zones to the east of Yalode. The overall ranges in elevation for the Urvara and Yalode Quadrangles are −5874 to 5671 m and −5819 to 5579 m, respectively.

HAMO color data (Fig. 2c) show subtle variations across the Urvara and Yalode Quadrangles. Smooth material, and basin floors in particular, exhibit more brownish colors and darker areas relative to the cratered terrain, which exhibits a mix of brown and blue colors. A number of impact craters (e.g., 23°S, 279°E; 54°S, 272°E; 48.9°S, 322.5°E; 25.8°S, 191.5°E; 39°S, 238°E; 34.3°S, 266°E) have distinctly blue ejecta materials. Bright ejecta deposits without the prominent blue color are observed surrounding craters centered at 21.2°S, 202.9°E and 42°S, 308.2°E, and dark brown crater materials are evident in the Yalode Quadrangle associated with Besua and an unnamed crater at 49°S, 301.5°E.

Survey orbit color composites (Fig. 2d) show significant variations across both quadrangles. Strong color variations are often associated with individual well-preserved ejecta blankets, which are apparent as bright blue regions. A large zone of deep red color is apparent within part of the Urvara basin floor and adjacent regions to the east, west, and south. Blue, tan, and brown colors characterize the northern parts of the two quadrangles. Color variations revealed by this composite image are difficult to interpret due to lack of clear correlation between color variations and morphologic or topographic features; however, they may indicate distinct mineral compositions, grain-sizes, or surface material ages, consistent with a complex geological history.

Fig. 3 shows geologic maps of the Urvara and Yalode Quadrangles of Ceres. The geologic unit and symbol scheme used was developed through iterative mapping as the Dawn spacecraft approached and orbited Ceres through the Survey, HAMO, and LAMO phases of the mission, and was refined through consultation and

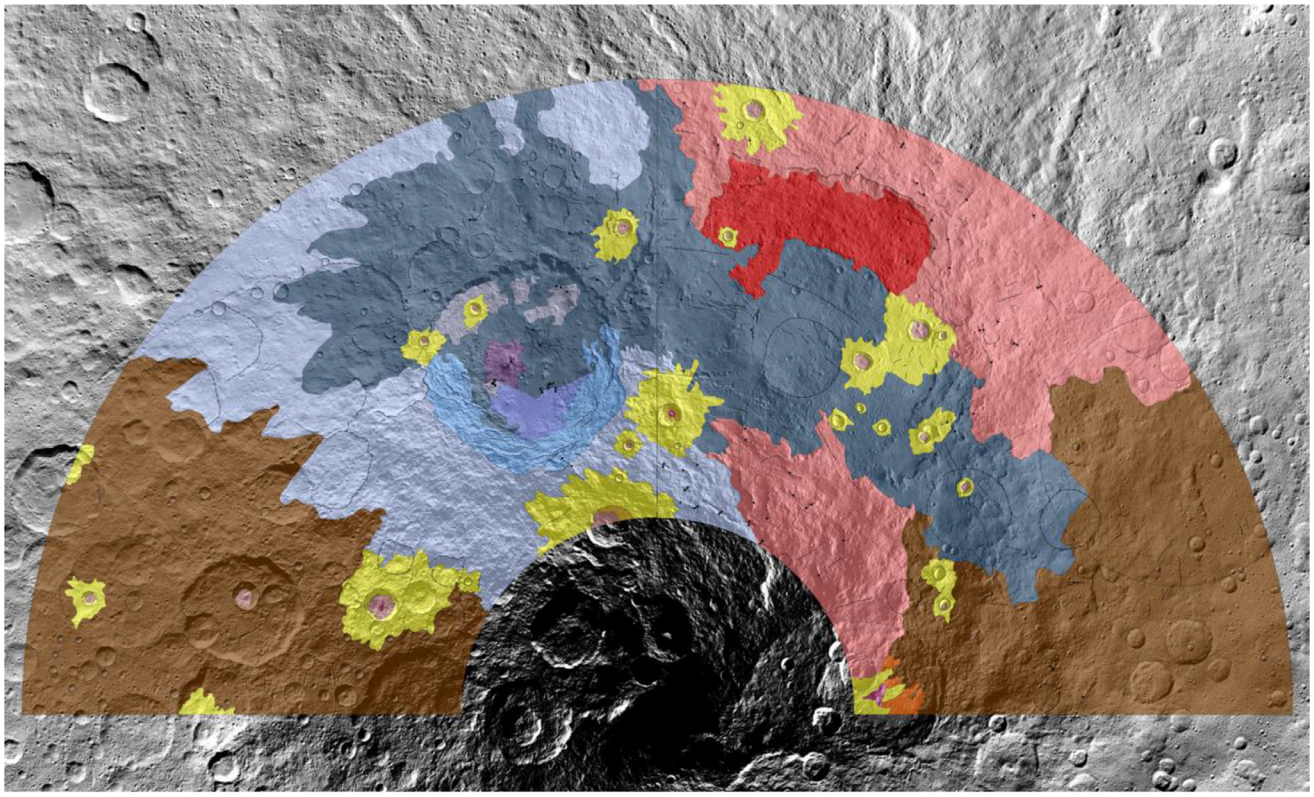

GEOLOGIC UNITS

Ue	Urvara ejecta material
Ut	Urvara terrace material
Ucp	Urvara central peak material
Ufs	Urvara floor material smooth
Ufh	Urvara floor material hummocky
UYs	Urvara/Yalode smooth material
Ye	Yalode ejecta material
Yfh	Yalode floor material hummocky
crt	cratered terrain
c	crater material
ct	crater terrace material
ccp	crater central peak material
cfs	crater floor material smooth
cfh	crater floor material hummocky

MAP SYMBOLS

- contact, accurate
- contact, approximate
- pit chain
- pit of impact crater floor
- raised rim of large impact crater
- raised rim of small impact crater
- buried impact crater rim
- channel
- degraded impact crater rim
- graben trace
- groove
- impact crater chain
- lobate scarp
- ridge crest
- scarp
- trough or narrow depression

Fig. 3. Combined geologic map of the Urvara (left) and Yalode (right) Quadrangles of Ceres. See Supplemental figures for individual Urvara and Yalode Quadrangle maps.

collaboration with other investigators conducting 1:500,000-scale geologic mapping of quadrangles on Ceres and the Dawn Science Team in general (e.g., Williams et al., 2017a). Consistent application of this geologic mapping approach allows comparison of 1:500,000-scale quadrangle maps (and their derived geologic histories) and facilitates integration of quadrangle maps into regional and global mapping efforts (Mest et al., 2016; 2017). Across the Urvara and Yalode Quadrangles, we have mapped 14 geologic units and 14 geologic feature types (including both line and point features). The main types of geologic units mapped include cratered terrain, Urvara and Yalode basin deposits (including smooth materials), and various types of impact crater materials.

4.1. Description of map units

The geology of the Yalode Quadrangle is dominated by the 260-km diameter impact basin Yalode and related crater materials extending to the northern and southern boundaries of the map region. Other named features include the impact craters Belun (33.7°S, 356.3°E, 36 km diameter), Besua (42.4°S, 300.2°E, 17 km diameter), Lono (36.7°S, 304.3°E, 20 km diameter), Mondamin (63.0°S, 353.6°E, 126 km diameter), and Tibong (29.8°S, 352.2°E, 36 km diameter) as well as Nar Sulcus (41.86°S, 280.11°E) and the eastern part of Baltay Catena (49.34°S, 274.49°E). The 170-km diameter impact basin Urvara and its extensive crater materials dominate the geology of the Urvara Quadrangle. Urvara impact deposits surround the basin on all sides and extend beyond the Urvara Quadrangle to the north, east, and south. Other named features in the Urvara Quadrangle include the impact craters Consus (20.7°S, 200.5°E, 64 km diameter), Fluusa (31.5°S, 277.9°E, 60 km diameter), Meanderi (40.9°S, 193.7°E, 103 km diameter), Sekhet (66.4°S, 254.9°E, 41 km diameter), and Tawals (39.06°S, 238.02°E, 8.8 km diameter), as well as four crater chains: Baltay Catena (49.34°S, 274.49°E); Gerber Catena (38.3°S, 215.5°E), Pongal Catena (37.37°S, 267.66°E), and the southernmost of the Samhain Catenae (2.75°S, 252.85°E). Geologic units identified in these quadrangles also occur elsewhere on Ceres (see other contributions to this volume), including the *cratered terrain* and a series of impact crater material units. Smooth material similar to that found elsewhere is also evident, but herein is grouped with basin materials because of its strong association to the Urvara and Yalode basins. We also identified and mapped geologic features, including structural and erosional features as well as those related to impact craters. Geologic contacts are typically not distinct and are generally mapped as approximate. The most well defined geologic contacts occur in association with the distal margins of lobate ejecta deposits associated with what appear to be pristine impact craters.

Cratered terrain (unit crt) is the oldest geologic unit identified in the Urvara and Yalode Quadrangles; it dominates the western portion of the Urvara Quadrangle and the eastern portion of the Yalode Quadrangle (Fig. 4). While generally exhibiting moderately rugged, heavily cratered surfaces, the cratered terrain exhibits variable morphology and includes smooth zones in which crater density and size is decreased relative to surrounding areas. Crater sizes in the two quadrangles range from the limits of LAMO resolution to the 260-km-diameter Yalode basin. Impact craters show a range in morphology from well preserved to highly degraded and/or buried forms. Much of the surface variability of the cratered terrain in both quadrangles can be attributed to local variations in the density, size range, and preservation state of impact craters. The rims of medium to large, relatively well-preserved craters have the greatest local relief. Localized concentrations of small impact craters may be due in some cases to clusters or chains of secondary craters. In addition to variations in the characteristics of the contained impact craters across cratered terrain surfaces, there are also significant changes in elevation within the cratered terrain.

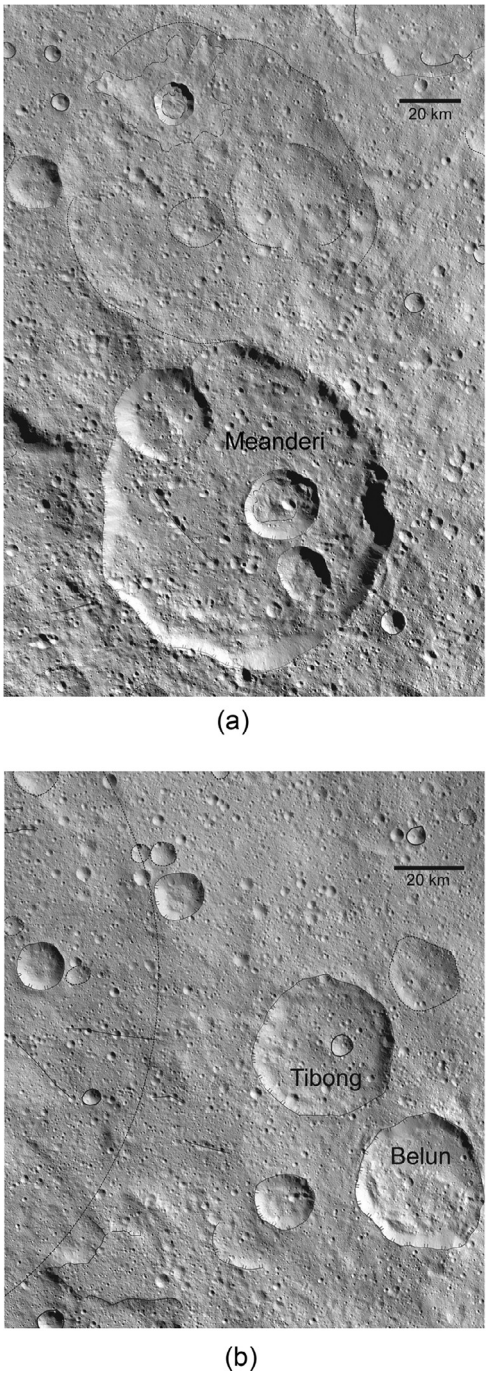

Fig. 4. Parts of LAMO mosaic showing cratered terrain of Ceres in Urvara (a) and Yalode (b) Quadrangles: a) cratered terrain to the west of Urvara showing craters exhibiting a range of sizes and degradation states, including 103 km diameter Meanderi and a similar-sized subdued basin to its north; image center is 34°S, 194°E, b) cratered terrain to the east of Yalode showing craters exhibiting a range of sizes and degradation states, including Tibong, Belun, and a segment of a degraded basin rim that extends into the Rongo Quadrangle; image center is 29.5°S, 349°E. Note also the small impact crater chains. Linework from geologic map (Fig. 3). North is to the top at center of both images.

There are smooth, low-lying regions that may delineate the interiors of ancient impact basins that have been eroded and/or buried (e.g., near ~26°S, 334°E in the Yalode Quadrangle and near ~36°S, 217°E in the Urvara Quadrangle). To the east of the Yalode basin there are also irregular high-standing zones not clearly associated with individual impact structures, although they roughly align to

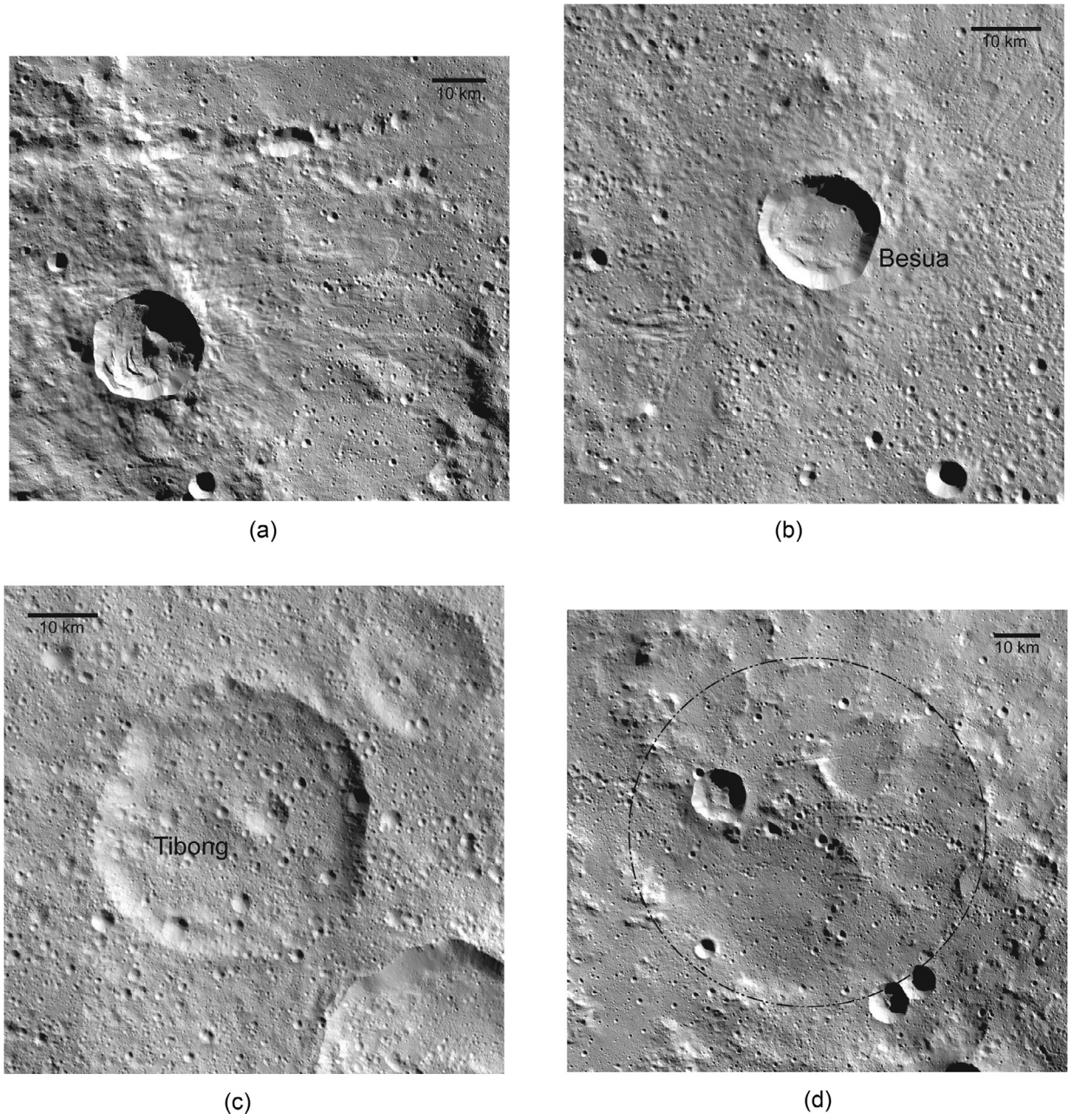

Fig. 5. Parts of LAMO mosaic showing range of impact crater morphologies in the Yalode Quadrangle: a) fresh crater with lobate ejecta and rim terraces; image center is 52.5°S, 276.5°E, b) Besua crater with smooth ejecta blanket and hummocky floor; image center is 42.5°S, 300°E, c) Tibong crater with degraded rim and heavily cratered floor; image center is 30°S, 352.5°E, and d) scarps and low hills aligned in circular pattern indicating buried/degraded crater rim in smooth material (outlined with buried impact crater rim symbol); image center is 45.5°S, 326.5°E. North is to the top at center of all images.

what may have been the southern rim of the degraded basin to the east of Yalode.

The cratered terrain in the Urvara and Yalode Quadrangles is interpreted to represent the ancient crustal materials of Ceres, dominated by crater materials from a multitude of impact events early in the history of the dwarf planet. The cratered terrain is likely dominated by ancient impact ejecta and crater wall and floor deposits, but may also include younger crater materials that cannot be clearly delineated and linked to a specific source crater.

Impact craters are observed throughout both quadrangles; they display a range of preservation states and have been mapped both within the cratered terrain and the widespread units associated with Urvara and Yalode (Figs. 5 and 6). Pristine features (including Tawals and unnamed craters on the northwestern rim of the Urvara basin and near the NW and SW corners of the Yalode Quadrangle) have sharply defined inner walls covered by talus and show lobate ejecta patterns that cover and mute the underlying terrains. Ejecta lobes are narrow and elongate to broad in planform and are observed to fill in topographic lows (such as troughs or crater chains) and can be deflected by local topographic obstacles (such as mounds or hills). At the southeastern corner of the Yalode Quadrangle, lobes of ejecta extending from a pristine crater in the Zadeni Quadrangle (Platz et al., 2016b; Williams et al., 2017a) appear to have been deflected around and partially over the central peak of Mondamin. The lobate ejecta blankets associated with pristine craters are often evident in color datasets. Other well-preserved craters in the region (including Urvara basin, 126-km Mondamin, 17-km Besua, 20-km Lono) have well-defined,

quasi-circular forms with prominent rims and in some cases discernible ejecta blankets. For example, Besua and Lono craters within the Yalode basin have recognizable ejecta blankets that have been mapped but the distal contacts of these deposits are difficult to identify as the ejecta deposits thin and merge with surrounding materials with distance from their source craters. Degraded impact features, including Yalode basin and numerous smaller craters, exhibit subdued rims, typically lack discrete ejecta deposits, and have infilled interiors. Some degraded craters within the cratered terrain (e.g., Tibong and Meanderi) have heavily cratered floor deposits. Crater floor deposits are generally hummocky and may include slump material from crater wall terraces as well as crater central peak material. Analyses of LAMO images and HAMO topography reveal the presence of remnant degraded and/or buried basin rims that indicate the dominant role of impact cratering throughout the geologic history of this region of Ceres.

Crater material units mapped in the Urvara and Yalode Quadrangles include *crater material (unit c), crater floor material hummocky (unit cfh), crater floor material smooth (unit cfs), crater terrace material (unit ct)*, and *crater central peak material (unit ccp)*. Crater material includes the ejecta and rim materials of well preserved to moderately degraded impact craters, as well as crater floor deposits in locations where the floor materials are not mapped as separate units. Some but not all craters with mappable ejecta blankets also exhibit hummocky floor deposits. In the Urvara Quadrangle, two unnamed craters exhibit both hummocky floor deposits and distinct, asymmetric lobate components in their ejecta. An unnamed crater to the southwest of Yalode with distinct ejecta shows well-developed interior terraces and a central peak. Mondamin crater contains smooth crater floor materials and a central peak. Central peaks are also evident in Urvara basin and two unnamed craters in the Urvara Quadrangle. Southern portions of the Urvara central peak complex exhibit clusters of overlapping round-to-irregular, low-rimmed depressions. These depressions may be degraded examples of pits observed in a variety of more pristine craters elsewhere on Ceres (e.g., Haulani, Ikapati, Dantu, and Kupalo), which are likely analogous to pitted crater materials previously identified on Vesta and Mars (Denevi et al., 2012; Tornebene et al., 2012; Sizemore et al., 2017).

The prominence and large areal extents of the Urvara and Yalode basins and associated deposits as well as their potential importance as stratigraphic markers in the geologic history of Ceres support distinguishing these basin materials from the rest of the impact crater materials in the two quadrangles. The impact crater deposits associated with the Urvara and Yalode basins have been mapped as basin materials, with similar sets of unit types as have been mapped for impact crater materials across the quadrangles. Mapping the different sets of Urvara and Yalode basin materials effectively defines geologic formations for each of the basins, although, as described below, a single unit of smooth material associated with the two basins is used.

Urvara and Yalode basins are distinct from one another in terms of morphology and preservation state. Yalode basin has a variably preserved rim, which is continuous and sharply defined to the north/northwest and is irregular or degraded elsewhere. Yalode's eastern rim is defined by a series of scarps and low hills aligned in a circumferential pattern. Hummocky deposits interior to a prominent scarp are observed along Yalode's northern rim and are mapped as *Yalode floor material hummocky (unit Yfh);* these deposits may be degraded terrace materials mixed with local mass-wasting and perhaps some ejecta from Urvara. The western rim of Yalode is disrupted by Urvara basin, and structural features extend from Urvara across Yalode's floor, including Baltay Catena. A series of roughly circumferential scarps delineate the structural trend of Yalode's western rim. The interior of Yalode basin contains an irregular ring of low hills that could represent a basin inner ring and/or reflect the presence of one or more subdued impact craters within Yalode. Large expanses of basin materials, mapped as *Yalode ejecta material* (*unit Ye*), are observed to the north and south of Yalode's rim and are interpreted to be the primary ejecta deposit from the Yalode impact event, perhaps mixed with some ejecta from Urvara. Within the Yalode Quadrangle and extending to the north into the Rongo Quadrangle (Platz et al., 2016b, 2016c; 2017), the Yalode ejecta material has a hummocky surface

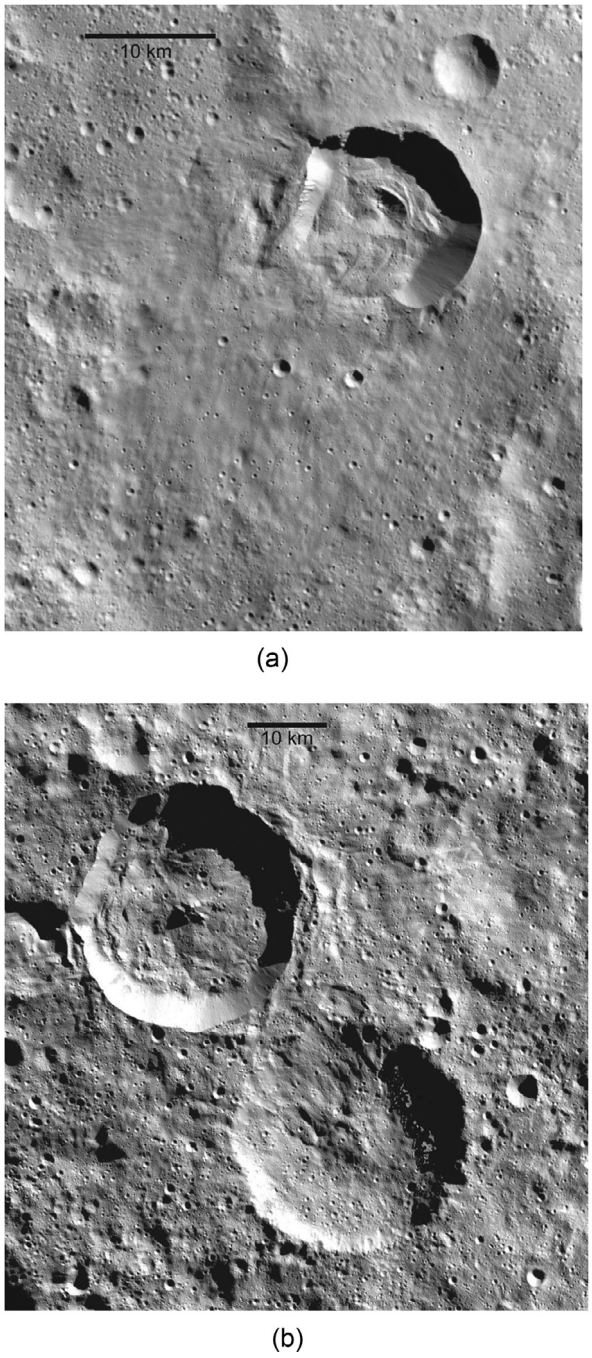

Fig. 6. Parts of LAMO mosaic showing examples of impact craters in the Urvara Quadrangle: a) fresh crater with a sharp eastern rim and hummocky floor material; image center is 35°S, 265°E. The western rim is collapsed, and ejecta to the northeast and collapsed rim material to the northwest exhibit localized lobate margins; b) The younger crater (top left) of two less pristine craters has a sharp rim, central peak, hummocky floor material, and lobate ejecta that overlies the older crater to the southeast; image center is 56°S, 204.5°E. North is to the top at center of both images.

that exhibits numerous surface features (e.g., scarps, ridges, and grooves) with dominant trends circumferential and radial to the basin and that contains numerous small impact craters. Medium and large craters are noticeably less abundant and where present more degraded/buried relative to those in the cratered terrain. The Yalode ejecta to the north of the basin and extending for ~150 km north displays a quasi-radial pattern in morphology and local relief/ruggedness that helps to define the spatial distribution of what may be the near-basin thicker and continuous ejecta materials. To the south, the Yalode ejecta is similarly hummocky and contains troughs, ridges, and scarps that are larger, although fewer in number and less clearly organized into radial or circumferential trends than to the north. Here, Yalode ejecta extends for 100+ km into the heavily cratered south polar region in the Zadeni Quadrangle (Platz et al., 2016b; Williams et al., 2017a), as well as across the cratered terrain to the southeast where it appears to have partially filled Mondamin. To the southwest, the Yalode basin and in particular Yalode ejecta material appear to be overlain by ejecta from the Urvara basin.

In contrast to Yalode, Urvara basin has a distinct central peak, consisting of a 20 km long east-west trending ridge. This ridge and surrounding high-standing, rugged terrain are mapped as *Urvara central peak material (unit Ucp).* Urvara also has a sharply defined rim that is continuous along its full circumference. Urvara exhibits a broad morphological dichotomy, largely due to extensive smooth materials covering the northern basin interior, and exterior regions to the north and east. These smooth areas are mapped as *Urvara/Yalode smooth material (UYs),* which is discussed in detail below. To the north and northeast, the Urvara rim consists of a single steep scarp bounding narrow muted terraces overlain by smooth material. The southern and western portions of the Urvara rim are rugged; the basin walls exhibit multiple broad interior terraces with rough surfaces, mapped as *Urvara terrace material (Ut).* Portions of the northern Urvara interior display a hummocky texture that disrupts extensive smooth material. These regions are mapped as *Urvara floor material hummocky (Ufh)* and are interpreted to be degraded terrace and wall-slump materials. The southernmost portion of the basin floor consists of smooth, dark, flat-lying material, mapped as *Urvara floor material smooth (Ufs).* This material exhibits a well-defined contact and localized embayment relationships with more broadly distributed smooth materials to the north and east. It also displays a lower small-crater density and distinct color relative to adjacent smooth materials. The origin of the Urvara floor material smooth unit is uncertain; on the basis of observed characteristics and geologic setting, hypotheses include localized extrusion of volatile-rich materials on the basin floor and remobilization of volatile-rich basin rim and/or terrace materials.

Like the rim and wall materials of Urvara, the crater materials external to the Urvara rim are morphologically dichotomous. Extensive rough-to-hummocky materials to the south and west are mapped as *Urvara ejecta material (unit Ue)* and interpreted to be part of the primary Urvara ejecta deposit. This unit also occurs along the northern boundary of the Urvara Quadrangle, although with a less rugged morphologic expression, and extends northward into the Occator Quadrangle (Buczkowski et al., 2107).

A large expanse of smooth material extends across the boundary between the Urvara and Yalode Quadrangles, which we map as *Urvara/Yalode smooth material (unit UYs)* (Fig. 7). Smooth material has been noted in a number of areas on the surface of Ceres; for example, smooth material is mapped on the floor of Kerwan basin and beyond its degraded rim and is interpreted to be the result of "impact-induced melting" of volatile-rich crustal materials (Williams et al., 2017b). Smooth material comprises a major portion of the floor deposits of the Urvara basin and a large region to the north and northeast of the Urvara rim inside the Urvara Quadrangle. This unit extends eastward, comprising much of the floor deposits of the Yalode basin, and continues across Yalode's eastern rim and beyond, finally forming the upper surface materials of some of the topographic highs outside of Yalode. Although the Urvara/Yalode smooth material displays some morphologic variability across its wide expanse, a combined basin unit was defined due to (1) the presence of smooth surfaces as its persistent and dominant characteristic and (2) a lack of distinct and traceable contacts that would suggest the need for subdivision.

Urvara/Yalode smooth material is identified in HAMO and LAMO mosaics based on relatively flat-lying and featureless surfaces. However, it is important to note that while smooth material is clearly less heavily cratered (and contains fewer large, degraded craters) than the cratered terrain, it contains large concentrations of small impact craters as well as some remnant crater rims from features that are presumably buried. We attribute some of the morphologic variability within the smooth material to differences in the sizes and abundance of small, superposed craters and also the presence of concentrations of secondary craters in clusters and chains. In particular, parts of the Yalode basin floor to the north and south/southeast appear to have higher crater densities. Nevertheless, the surface materials are smooth in and around these areas and clear contacts are not evident. Surface morphology within the Urvara/Yalode smooth material also appears to vary due to the nature of the underlying terrain. Smooth material is interpreted to drape and bury pre-existing terrain such that where rugged underlying topography exists, it gives the smooth materials a more hummocky and irregular appearance. For example, smooth material is observed to cover mesas and knobs that represent the degraded western and eastern rims of Yalode basin. Similarly, smooth material covers portions of the northern and eastern rim and interior walls of Urvara.

Urvara/Yalode smooth material is found on some of the lowest and flattest surfaces in both quadrangles (i.e., the floors of the Urvara and Yalode basins); however, the distribution of smooth material does not correlate with either local or regional topography. Smooth surfaces cover local topographic highs (including the Urvara and Yalode rims and the Yalode interior ring structure) and extend onto the highest surfaces in the Yalode Quadrangle. Contacts between the cratered terrain and smooth material are typically not distinct, but the smooth material does superpose the cratered terrain. Based on this superposition relationship, the distribution of smooth material, and its lack of correlation with topography, the Urvara/Yalode smooth material is interpreted to be a combination of deposits from both impact events that have merged together to form a single unit. This unit would have variable thickness revealing the ruggedness of the underlying terrain to different degrees as well as a variable impact crater density due to crater chains, secondary clusters, medium-sized (~2–5 km in diameter) impact craters and the age difference between the Urvara and Yalode impact events. Smooth material on the Yalode basin floor would presumably be dominated by Urvara ejecta and the more easterly deposits would contain greater abundances of Yalode impact deposits. This interpretation is supported by the qualitative observations of crater density discussed above and crater retention ages derived for parts of the two quadrangles (See Geologic History section). The coalescence of deposits related to the two basins, as well as perhaps other smaller craters, could have been facilitated by the inclusion of water ice in the impact deposits. This hypothesis is consistent with the lack of clear definition of contacts for ejecta deposits associated with all but the youngest impact craters. Continued modification of the surface by small impacts also could have contributed to obscuring contacts between parts of the unit derived from different sources.

The distribution of smooth material may have once been more widespread in the Yalode Quadrangle, with the thinner outlying

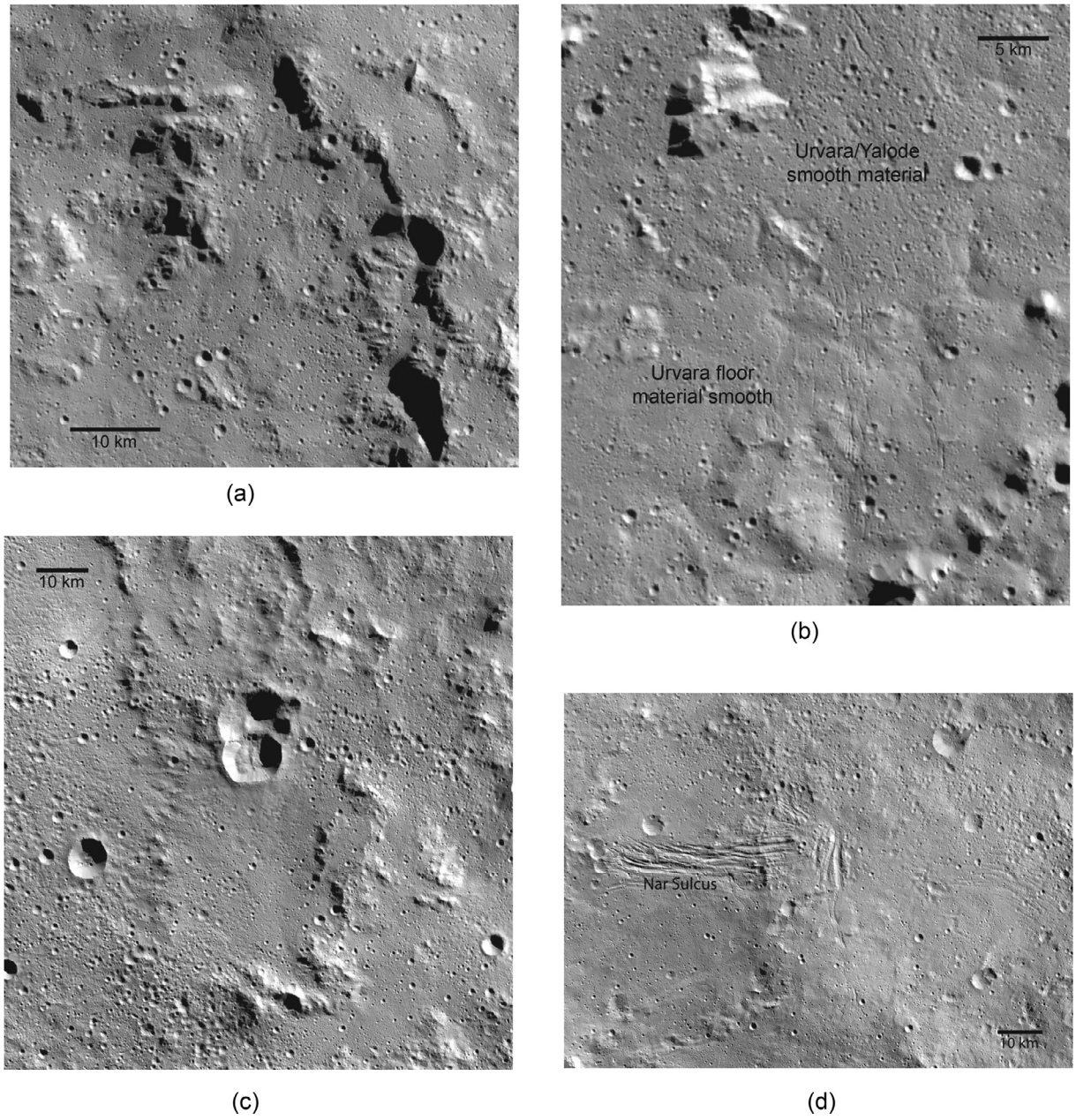

Fig. 7. Parts of LAMO mosaic showing examples of smooth material in the Urvara and Yalode Quadrangles: a) Urvara/Yalode smooth material on the eastern rim of the Urvara basin; image center is 41°S, 259.5°E, b) contact between Urvara/Yalode smooth material and Urvara floor material smooth on Urvara basin floor; image center is 49.5°S, 253°E, c) Urvara/Yalode smooth material across the degraded eastern rim of Yalode basin; smooth material appears to cover scarp-bounded mesas (southeast of center) that are remnants of the basin rim; image center is 45.5°S, 314.5°E, d) Urvara/Yalode smooth material in the interior of Yalode basin and surrounding Nar Sulcus; image center is 42.5°S, 283.5°E. Note that both the structural fabric (of Nar Sulcus and to east) and impact crater chains have E-W trends that are radial to the Urvara basin. North is to the top at center of all images.

deposits becoming incorporated into the cratered terrain and other basin ejecta materials. Note that the smooth material may be a specific type of basin ejecta deposit, representing excavation of a distinct type of substrate and/or a segregation of less-rocky ejecta materials from the primary ejecta during emplacement. Evidence for excavation of a distinct substrate is most apparent in the Urvara Quadrangle, where the distribution of smooth material suggests that much of it was deposited as fluidized ejecta to the north of the Urvara rim and on the basin floor (post-impact modification may have also played a role in the Urvara floor). The distinctly different texture of the Urvara ejecta deposits mapped to the south of the basin and in extended outlying regions suggests that the Urvara impactor may have encountered a heterogeneous target.

Current knowledge of Ceres (as discussed in the Background section) suggests that the Urvara and Yalode impacts, as well as other crater-forming events, may have excavated or exposed relatively weak crustal materials due to enrichment in ices, phyllosilicates, and/or salts. This is supported by observations of surface morphology in the Urvara and Yalode Quadrangles, including widespread smooth surfaces, the presence of some lobate margins, the gradational nature of ejecta contacts, and inference of coalescence of multiple deposits to form the Urvara/Yalode smooth material. Localized extrusions of ice-rich materials within the area encompassed by Urvara/Yalode smooth material are consistent with surface characteristics and could play a minor role in formation of this unit.

4.2. Geologic features

Based on observations of the Urvara and Yalode Quadrangles in LAMO images, a variety of linear and point features have been mapped to illustrate geologic characteristics that help to convey processes that have affected this part of the surface of Ceres. Many of the map symbols used relate to impact crater processes. Impact crater rims are mapped for large (10 km and larger) and small (5–10 km in diameter) craters with well-defined rims. Degraded and buried rims are also identified with different symbols. Buried craters are particularly noticeable within the Urvara/Yalode smooth material, suggesting that they formed on pre-existing surfaces and have been covered by smooth material. Pits on impact crater floors have been identified and mapped within Urvara basin (Sizemore et al., 2016a). Numerous impact crater chains are evident scattered throughout both the Urvara and Yalode Quadrangles. Impact crater chains typically consist of a linear to curvilinear, elongate grouping of relatively small impact craters, although crater size can vary within a given chain. Baltay Catena is a chain of significantly larger craters that extends eastward from a scarp-bounded trough radial to Urvara (Fig. 8a). Pongal Catena has similar morphology and is a curvilinear feature composed of a proximal trough with a distal chain of craters extending radially from Urvara to the northeast (Fig. 8a). Impact crater chains have typical lengths of ~10–~30 km and can be as long at 100 km. The orientations of impact crater chains are variable but a significant number, particularly in the Urvara/Yalode smooth material, appear to be radial to Urvara.

Two long pit chains, one of the Samhain Catenae and Gerber Catena (~126 and ~143 km, respectively), trend in a quasi-radial pattern northwest of Urvara (Fig. 8b). These are distinguished from impact crater chains because the contained pits do not exhibit raised rims and are elongate in planform along the trend of each catena. Other features mapped across the region include scarps, ridges, troughs, graben, grooves, and channels. Scarps oriented in a circumferential pattern reveal terrace blocks along the southern interior rim of Urvara, and scarp-bounded troughs extend radially from the basin to the north and east. Scarps delineate both the relatively continuous northern rim of Yalode as well as small blocks and mesas that define remnants of Yalode's degraded and discontinuous rims to the northwest and east (Fig. 7c). Scarps are also observed within Urvara and Yalode ejecta materials and the cratered terrain. Lobate scarps are mapped to identify lower relief and more arcuate scarp features observed in Urvara/Yalode smooth material (and to distinguish them from scarps associated directly with basin rim features). Throughout the two-quadrangle map area, ridge and trough symbols are used to identify elongate topographic features that provide ruggedness to the landscape on a local scale. Ridges and troughs are abundant in ejecta material to both the north and south of the Yalode basin and may represent some combination of topographic features blanketed by ejecta, structural features resulting from the large Yalode and Urvara impacts, and the patterns of ejecta emplacement.

A few small graben are evident in the Urvara/Yalode smooth material on the Yalode basin floor and in the cratered terrain to the east of Yalode. These features are typically ~10 km in length, are shallow, and have constant widths. The eastern examples seem to be associated with a degraded impact crater. The graben on Yalode's floor are found along the inner edge of a mound that includes the highest elevation interior to Yalode's rim and that forms part of the irregular inner ring of hills in Yalode's interior. Also associated with this mound is a high concentration of grooves and some channels (Fig. 9a). Grooves in the Urvara and Yalode Quadrangles are shallow, linear to curvilinear troughs that often occur in closely spaced, parallel to sub-parallel sets. Channels are narrower, shallower, and typically shorter than grooves and have curvilinear to sinuous planforms. Channels may have variable widths and in some cases two channel segments may exhibit junctions, forming immature or proto-networks. Channels are observed to follow the local slope direction, including adjacent to the inner ring of Yalode and along Yalode's southern rim (Fig. 9).

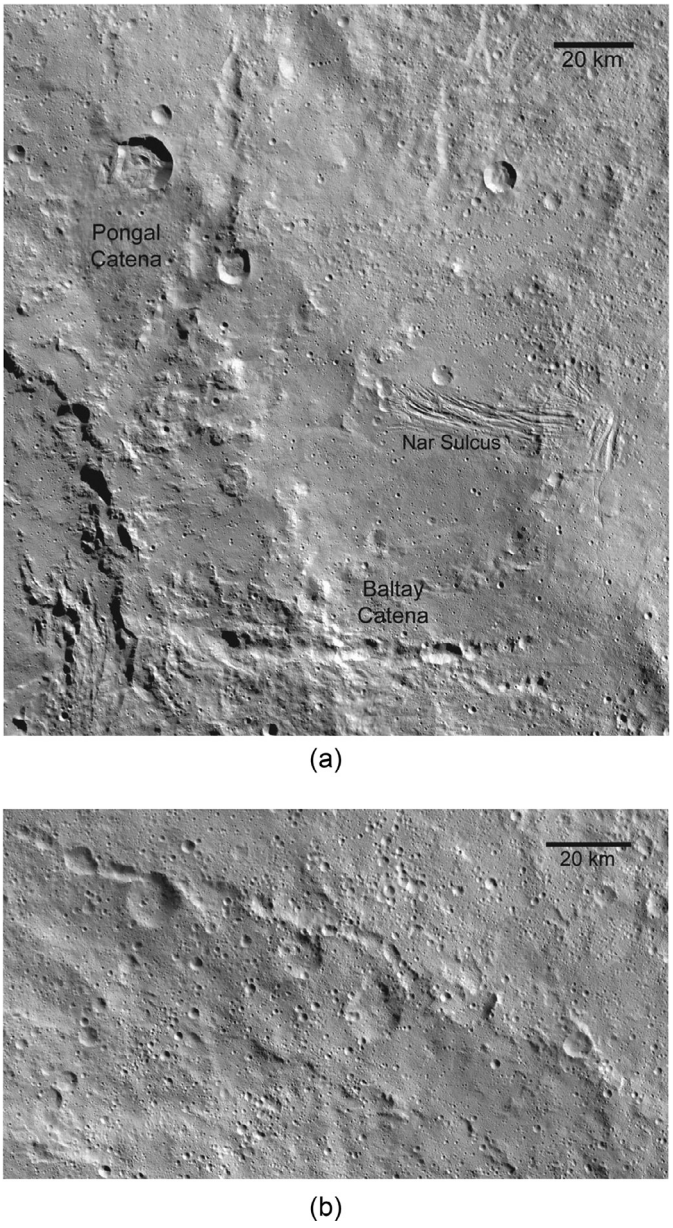

Fig. 8. Parts of LAMO mosaic showing prominent catenae in the Urvara-Yalode region: a) Pongal and Baltay Catenae; image center is 40°S, 273°E, b) southernmost member of the Samhain Catenae group; image center is 26.5°S, 227.5°E. Pongal and Baltay Catenae are curvilinear and transition from trough-like structures near the eastern rim of Urvara to series of distinct rimmed depressions at their distal ends. This may indicate an origin as secondary crater chains. In contrast, the Samhain Catenae to the west of Urvara and Gerber Catena (not pictured) are more linear and consist of elongated, rimless pits. North is to the top at center of both images.

In the Urvara Quadrangle, grooves are predominantly found in Urvara/Yalode smooth material but also occur in Urvara ejecta and Urvara terrace materials. Channels typically occur in association with grooves in Urvara/Yalode smooth material, but can also be seen in Urvara hummocky and smooth floor materials (Fig. 10). In the Yalode Quadrangle, grooves and channels occur together in Urvara/Yalode smooth material, Yalode ejecta, and on the ejecta blanket of the crater Lono. Grooves oriented in approximately an

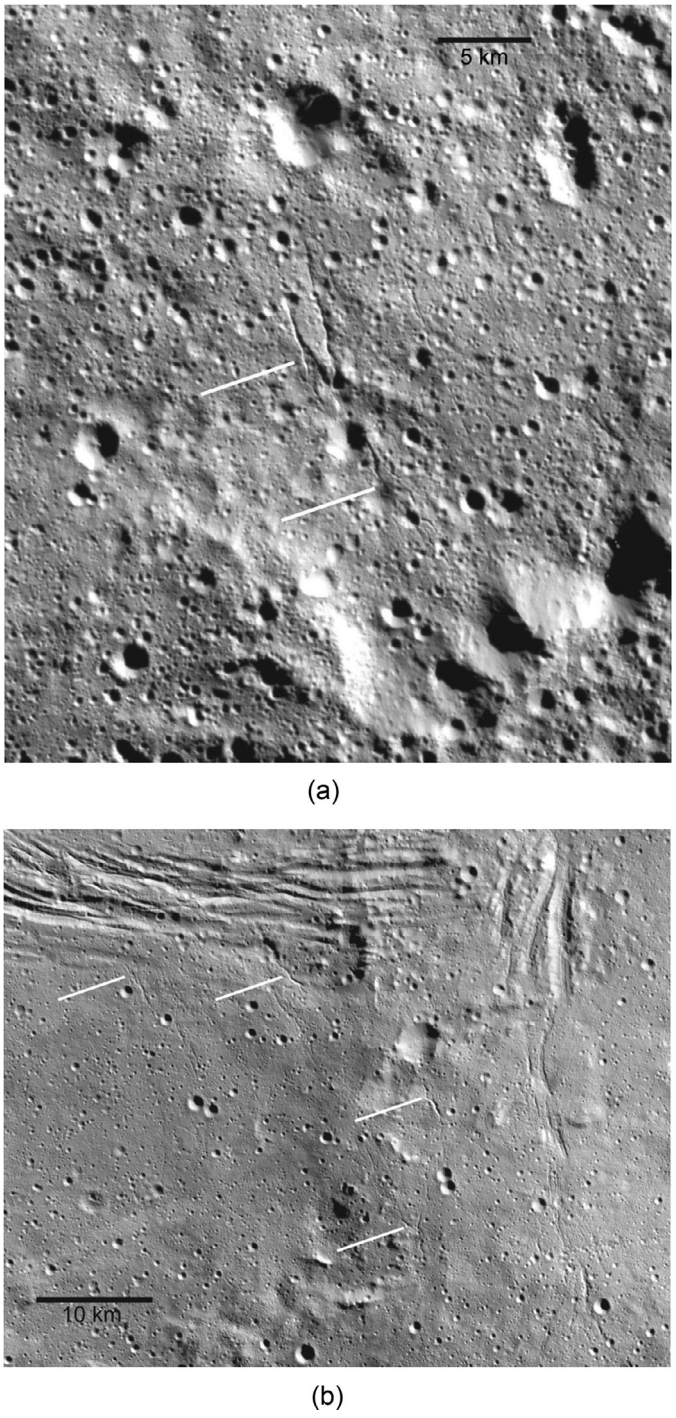

Fig. 9. Parts of LAMO mosaic showing channels within smooth materials. Along Yalode basin's rim (Fig. 9a; image center 53°S, 257°E) and inner hills (Fig. 9b; image center 44°S, 280.5°E), small, narrow channels (some examples noted by white lines) that may be aligned with structural trends dissect smooth materials. In some cases, channel segments form tributary patterns that extend along local slopes. Channel morphology suggests a complex sequence that may include extension and related collapse, perhaps followed by localized sapping and flow. North is to the top at center of both images.

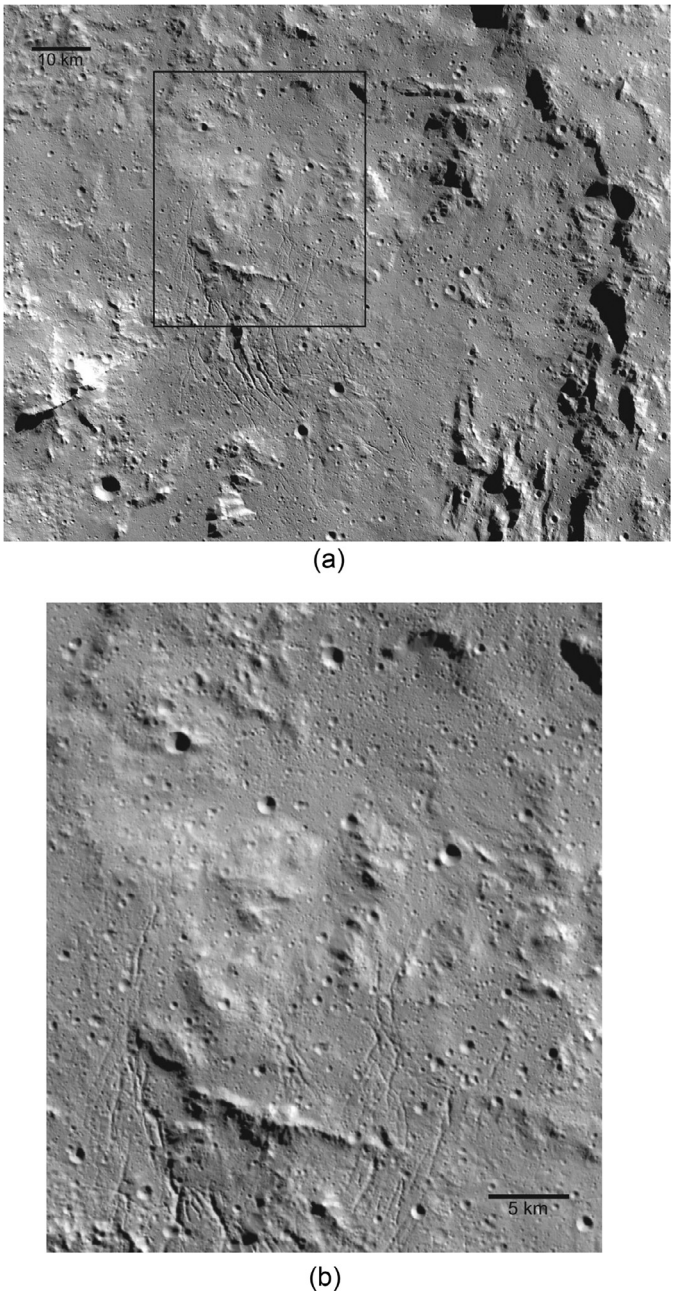

Fig. 10. Parts of LAMO mosaic showing features on the Urvara basin floor: a) prominent complex of grooves and ridges situated between the central peak complex and the eastern basin rim; image center is 42.5°S, 255°E. Pitted areas to the south of the central peak are also visible (bottom right). b) detail of grooves and channels in a hummocky region to the northeast of the ridge/groove complex; image center is 41.5°S, 253°E. Channels and grooves in this location are associated with sinuous forms that extend out of hummocky region to the northeast, suggesting downslope movement of smooth material. North is to the top at center of both images.

east-west pattern are evident north of Urvara in ejecta and smooth material, along the northern rim of Yalode, and in Yalode's ejecta north of the basin. These appear to be part of a textural fabric of the surface materials that also show impact crater chains in this orientation and are attributed to impact sculpting of the surface and/or settling of surface materials. Prominent concentrations of grooves and channels are found adjacent to Urvara's central peak in smooth material and within smooth materials on Yalode's floor.

The western part of the ring of high-standing hills on Yalode's floor displays a high concentration of geologic features of various types and orientations, which are referred to collectively as Nar Sulcus (Figs. 7d, 8a, 9b). A closely-spaced set of roughly east-west trending grooves extends from lower-lying smooth materials inward of Yalode's degraded western rim into the hills of the inner ring; this trend continues with an additional set of grooves to the

west of Besua crater. North-trending graben generally oriented perpendicular to the grooves are observed in smooth material on the inner edge of Yalode's inner ring. Channels oriented approximately north-south and following local slopes are evident within this area (Fig. 9b). The overall combination of features suggests a zone of focused deformation/disruption of the surface materials followed by localized incision due to small-scale collapse and possible migration of volatiles under, through, or across the surface materials.

Lono crater also exhibits sets of grooves in its ejecta that extend to the northeast and southwest. Grooves of the northeast set occur in closely spaced sets and are generally short. Grooves to the southwest are longer, curvilinear features that give the ejecta blanket a dissected appearance. To the northeast of Lono, the floor and rim of a buried impact cater within Yalode ejecta displays grooves and a few channel forms in a pattern that follows the rim of Yalode, connecting scarp-bounded mesas south of Lono to ridges and scarps of Yalode's northern rim.

A prominent system of ridges and grooves is located on the Urvara floor, east of the central peak complex (Fig. 10). Two of the ridges and a subset of the grooves run in parallel, trending N-S within Urvara/Yalode smooth material (UYs). Grooves in this subset are linear, and typically wider and deeper than elsewhere in Urvara. Small channels are also present, mostly trending N-S near the center of the complex. At the northern edge of this area, a third ridge runs NW-SE, with a second subset of grooves running perpendicular to it (NE-SW). To the northeast, this second set of grooves becomes more branching and sinuous, transitioning to channels in a region mapped as Ufh (Fig. 10b). These channels terminate to the NE in an area where small-scale streamlining suggests downslope motion and settling of smooth material.

5. Characteristics of impact basins on Ceres: insights from Urvara and Yalode

Dawn Framing Camera datasets have been used to examine the morphology, morphometry, spatial distribution, and size frequency of impact craters on the surface of Ceres over sizes of a few kilometers in diameter and larger (Bland et al., 2016; Hiesinger et al., 2016; Marchi et al., 2016). Ceres has a heavily cratered surface with a heterogeneous crater distribution attributed to the effects of spatial variations in the ice-rock crust and impact-induced resurfacing. The transition diameter from simple to complex craters (~7.5–12 km) adjusted for surface gravity follows the trend of icy moons in the outer solar system (Hiesinger et al., 2016). Smooth deposits commonly seen on the floors of craters with diameters greater than 40 km are attributed to mobilization of impact melt, impact-induced volcanism, or post-impact melting, and the fractures and central pits observed indicate a weak substrate relative to the Moon and Vesta (Hiesinger et al., 2016). There is limited evidence for relaxation at long wavelengths. For example, Kerwan exhibits a relaxed profile, whereas other large basins (including Urvara and Yalode) show greater depths than predicted in relaxation profiles (Bland et al., 2016). HAMO DTMs from stereo-photogrammetry show that Urvara has an apparent depth (depth relative to the surrounding terrain) of 7 km (range 5–9 km) and Yalode has an apparent depth of 6.5 km (range 2.5–8.5) (Bland et al., 2016). There is an apparent absence of craters greater than 300 km in diameter and a general depletion in large craters across the surface of Ceres (Hiesinger et al., 2016; Marchi et al., 2016), with the lower crater densities in the southern hemisphere thought to be due to resurfacing associated with the Urvara and Yalode impacts.

The general characteristics of the Urvara and Yalode basins have been described above in conjunction with definition of geologic units for 1:500,000-scale quadrangle mapping on Ceres. Dawn datasets provide views of Ceres that for the first time allow us to apply its surface geology to broaden our understanding of the nature and diversity of impact processes. Here we use Urvara and Yalode as examples to explore the morphologic attributes of impact basins on Ceres and to explore the use of impact basins as stratigraphic markers for the geologic history of Ceres.

Urvara and Yalode are adjacent impact structures and part of a grouping of three large basins in the southern hemisphere of Ceres. A degraded impact basin that predates the formation of Yalode is evident to the east of Yalode based on the presence of a quasi-circular depression and the presence of degraded remnants of its rim (particularly evident in the Rongo Quadrangle). Yalode is a roughly circular structure with a variably preserved rim and irregular inner ring. Urvara is a well-defined circular basin with a central peak and rim zones defined by scarps and terracing.

Both Urvara and Yalode display morphologic differences along their rims, and their rims have different properties when compared to each other. Urvara's well-defined rim consists of a singular steep scarp to the north and a complex of concentric terraces to the south and west. The rim to the northeast is composed of a series of hills aligned in a basin-concentric pattern with steep scarps facing the basin interior. These characteristics show that the inner crater rim (or wall) is well defined, and gives definition to the basin as a whole, but there is no significant expression of the outer part of the rim. This is in contrast to other craters on Ceres that show morphologic and topographic signatures for both the inner and outer crater rims. For example, Occator crater (92 km diameter; 19.8°N, 239.3°E) (e.g., Buczkowski et al., 2017; Nathues et al., 2017) to the north of Urvara exhibits significant terracing along its inner crater walls and also displays both inner and outer crater wall slopes; the inner rim is predominantly characterized by steep and well-defined scarps, whereas the outer rim is a more subtle annular mound of materials that extend outward from the crater. In one location along Occator's wall to the east, the rim is defined only by terracing. By comparison with Urvara, this suggests that either 1) in some cases crater rims on Ceres are not constructed by deposition of an overturned flap and the crater margin is defined simply by collapse and terrace formation or 2) the presently observed crater rims defined predominantly by scarps suggest significant enlargement of crater structures such that much or all of the original rim has been modified or destroyed.

Yalode's rim to the north consists of a singular steep scarp similar to that of Urvara. The remainder of Yalode's rim is not well defined. To the south it can only be inferred based on the transition from Urvara/Yalode smooth material to the more rugged Yalode ejecta and the change in topography associated with that transition. To the east, Yalode's rim consists of basin-concentric hills and mounds with scarps on their basin-interior margins. To the northwest, the rim is expressed as a zone with numerous small (both in length and exposed relief) scarps with variable but generally basin-concentric orientations. The western rim is largely non-existent; the series of low-relief hills observed between Urvara and Yalode may include remnants of both basins' rims. Hummocky floor deposits adjacent to Yalode's northern rim are interpreted to be some combination of degraded terraces and local mass-wasting deposits, perhaps mixed with some Urvara ejecta. Hummocky floor materials are also observed in patches interior to Urvara's northern rim. Comparisons between Urvara and Yalode and to other craters on Ceres such as Occator indicate a potential evolution in inner rim morphology over time from a) well-defined terraces to b) a combination of degraded terraces and adjacent hummocky deposits to c) more subdued but still hummocky floor materials with progressive degradation. However, diversity in degradational sequences, perhaps related to substrate properties, is also apparent. For example, Kerwan basin is defined by a degraded rim (with inner and outer rim slopes) but exhibits no terraces; the same morphology is evident along the northern rim of the degraded basin to the east of Yalode.

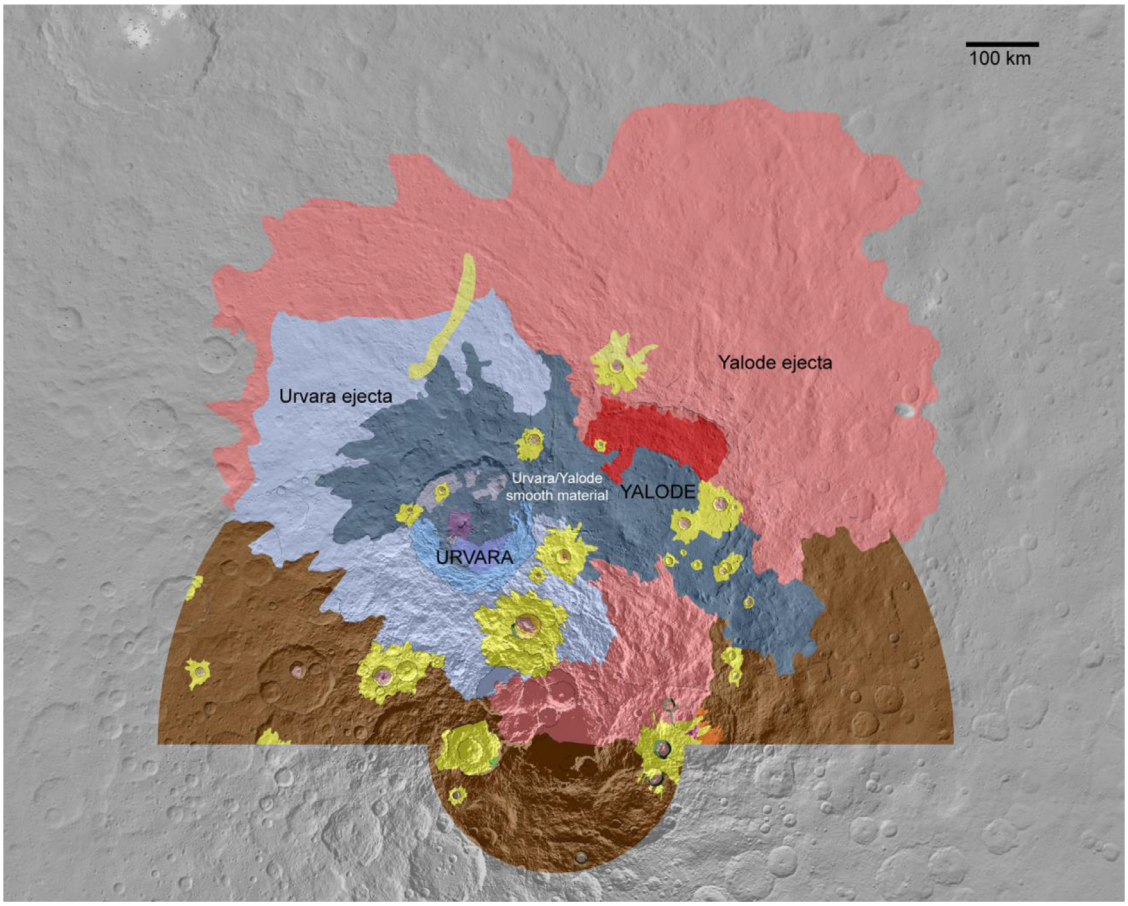

Fig. 11. Geologic maps of the Urvara, Yalode, and Zadeni Quadrangles of Ceres showing the mapped extents of Urvara and Yalode ejecta deposits along with contacts of these units from the Occator (Buczkowski et al., 2017) and Rongo (Platz et al., 2016b, 2016c; 2017) Quadrangles to the north. Zadeni Quadrangle from Williams et al. (2017a). Polar stereographic projection centered on 270°E. (For interpretation of the references to color in this figure legend, the reader is referred to the web version of this article.)

Numerous catenae have been identified on the surface of Ceres and many of these features are spatially associated with the Urvara and Yalode basins. Pongal and Baltay Catenae extend radially from Urvara to the northeast and east, respectively, and we interpret these to be large impact crater chains. Baltay Catena dissects Yalode floor deposits and thus clearly shows the younger relative age of Urvara. Uhola Catenae extend north from near the northern rim of Yalode and consist of chains of large troughs and elongated pits. A prominent western feature is radial to Yalode but the prominent feature to the east is parallel to the first, suggesting that the Uhola Catenae in general are not radial to Yalode. Samhain Catenae include a large number of pit chains with northwest-southeast trends that extend across a large area of Ceres' surface north of Urvara and Yalode. The southernmost of the Samhain Catenae and Gerber Catena are radial to Urvara. The Samhain Catenae have been interpreted to be tectonic features that pre-date the formation the Urvara and Yalode impacts (Buczkowski et al., 2016; Marchi et al., 2016; Scully et al., 2016a,b). Our observations of these features do not show clear burial by Urvara and Yalode ejecta, suggesting formation may not have preceded basin formation. Junina Catenae are secondary crater chains to the west of Occator crater (up to ~500 km from the rims of Urvara and Yalode) that are believed to be associated with Urvara and/or Yalode; their non-radial trends to the basins are attributed to Ceres' fast rotation and small radius (Scully et al., 2016b). Some of the catenae near Urvara and Yalode occur in ejecta materials from these basins but others are observed to extend beyond mapped ejecta deposits.

Fig. 11 shows LAMO-based geologic mapping results for the Urvara and Yalode basins. This composite from five 1:500,000 quadrangles shows the extent of mapped ejecta deposits and the boundaries between Urvara and Yalode ejecta. As discussed above, geologic features in the region that may be basin-related extend beyond the distal edges of the mapped ejecta, suggesting that the effects of basin formation on the surface of Ceres are far-reaching. Precise locations of geologic contacts for the Urvara and Yalode ejecta deposits are difficult to determine and map. Geologic contacts on Ceres are typically indistinct except for young crater materials, and the emplacement of distal ejecta by its very nature suggests thinning outward and merging gradually into the surrounding cratered terrain. Global mapping using HAMO data by Mest et al. (2016, 2017; see also Buczkowski et al., 2016) shows a similar distribution of ejecta surrounding Urvara and Yalode for the most part, but more extensive ejecta deposits to the east and south of Yalode than from LAMO-based mapping.

The spatial distributions of ejecta deposits, crater chains, and basin-related structural features associated with Urvara and Yalode have the potential to provide important stratigraphic constraints for deciphering Ceres' geologic history, even with the present uncertainties in ejecta distribution and thickness and the exact mode(s) of formation of linear features. To examine possible theoretical bounding extents for Urvara and Yalode ejecta, we present simulations of the distribution and impact velocity of ejecta for each of the basins. For these simulations, we assumed a 45° ejection angle for each test particle and a symmetric ejection geometry, and utilized ejecta scaling laws described in Housen and Hol-

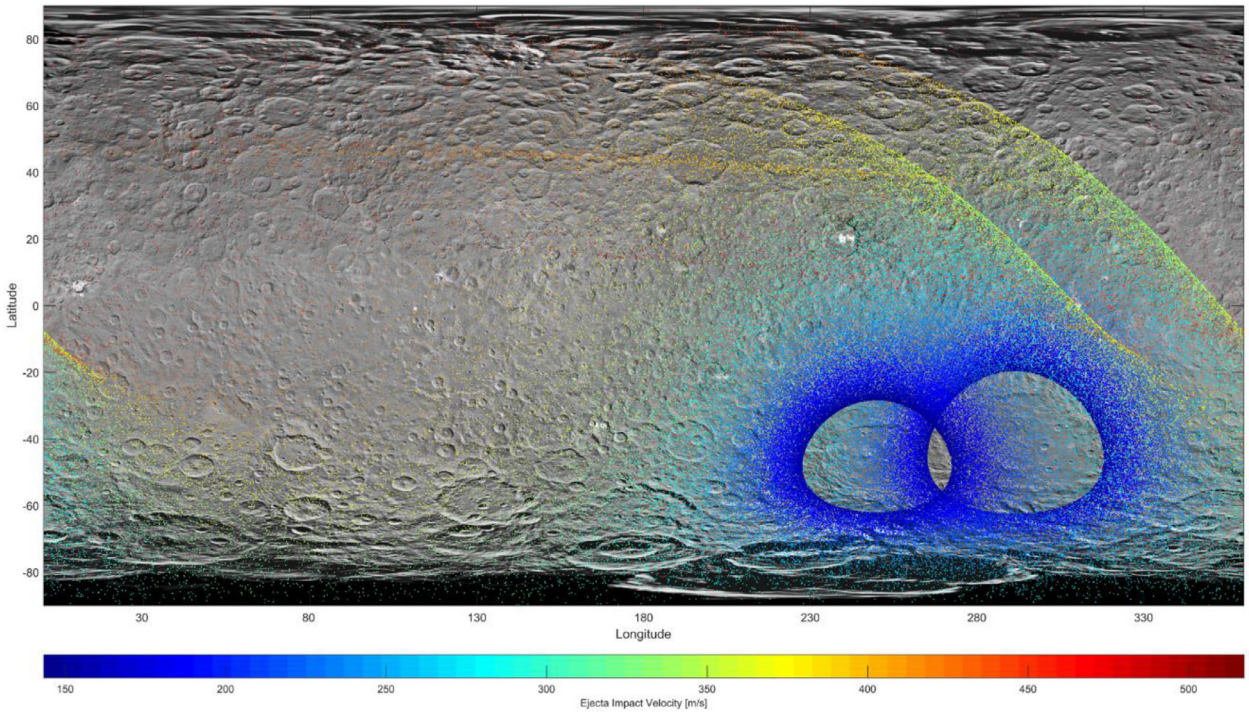

Fig. 12. Global mosaic of Ceres centered at 180° longitude. Colored points represent the impact locations of ejecta tracer particles from the Yalode and Urvara impact events. The color encodes the impact velocity of each particle. The particle density is a measure of the relative probability that secondary craters could have formed. Yalode particles inside Urvara crater may be ignored, since the later formation of Urvara resurfaced that area. (For interpretation of the references to color in this figure legend, the reader is referred to the web version of this article.)

sapple (2011). Ceres' rotation and ellipsoidal shape were taken into account, though changes in the gravity field due to mass redistribution during the impact were not. Results are shown in Fig. 12. Deep blue dots represent the slowest ejecta able to form secondary craters (~200 m/s (Bierhaus et al., 2012)); the continuous ejecta blanket would occur within this deep blue zone, which aligns well with mapping results to the north of Yalode, where rugged terrain interpreted as the continuous ejecta blanket is observed. Based on this simulation, continuous ejecta would be expected to appear roughly within one crater radius around Urvara and Yalode, but deposition of ejecta would occur at significantly greater distances (i.e., one crater diameter and farther). Based on these simulations we would also expect that some linear features (e.g., crater chains) associated with the Urvara and Yalode impact events may not be oriented radial to these basins due to Ceres' rotation.

In addition, we can make comparisons to large impact structures on other small, airless, rocky bodies in order to better understand the potential nature and extent of effects from the Urvara and Yalode impact events on Ceres' surface geology. This is useful for assessing the geologic records of these basins as both regional and global stratigraphic markers. Numerous variables come into play during and after an impact event and thus influence the characteristics of the resulting crater; such variables include the parent body's gravity and rotation, the physical properties of the body, the physical properties of the impactor, and the conditions at impact (e.g., Melosh, 1996). Modeling each of these individually is beyond the scope of this mapping effort. However, it is instructive to compare quantitative characteristics among the largest basins on different bodies to provide context for understanding basins on Ceres (Table 1).

Yalode basin, at 260 km diameter, measures ~9% of Ceres' circumference (assuming a geometric mean radius of 469.7 km (Russell et al., 2016)). In comparison, the lunar Imbrium basin, with a diameter of ~1145 km (e.g., Wilhelms, 1987), is ~10% of the Moon's circumference (assuming a 3475 km lunar diameter). The Apollo 16 site, 1600 km from the basin rim, is widely considered as influenced by Imbrium ejecta (e.g., Wilhelms, 1987). Basin formation modeling has indicated that Imbrium ejecta may occur up to distances of three basin diameters (e.g., Housen et al., 1983; Haskin et al., 2003) and mix to depths of 100 s of meters even 600–700 km from the basin rim (Petro and Pieters, 2008). Similarly, the Orientale basin, at 930 km, is ~9% of the Moon's circumference. The Hevelius Formation, which defines the continuous ejecta blanket of Orientale, extends from 300–600 km from the ring defined by Montes Cordillera (Scott et al., 1977); recent work tying the formation of light plains to the Orientale impact suggests that the influence of Orientale actually extends up to four basin radii away (1800 km, or 17% of the lunar circumference) (Meyer et al., 2016).

We examined various characteristics of impact basins on the Moon, Mercury, Callisto, Vesta, and Ceres to better assess how the inferred extents of ejecta and basin-related features (e.g., crater chains and circumferential fractures and ridges) on Ceres compare to other bodies with a broad range of physical properties (Table 1). Urvara and Yalode are of similar size in relation to the size of their parent body as large basins on the Moon and Mercury. We evaluated the extent of the influence of a basin on its host planetary surface by examining the extent of observed/mapped ejecta and identification of the distances at which basin-related features are recognized. Values were compared among planetary bodies by normalizing to crater diameter. Ranges in values (if given) extend from low, as defined by the extent of ejecta, to high, based on extent of basin-related features. The ranges for Urvara (2.5–3.4) and Yalode (2.1–2.8) are generally comparable to those of the other planetary bodies shown but most similar to those of the Asgard and Valhalla basins on Callisto. These results are also consistent with the simulation results shown in Fig. 12. The simulation re-

Table 1
Characteristics of large impact basins.

Impact Feature	Parent Body	Crater Diameter[a] (km)	Parent Body Diameter[b] (km)	Parent Body Circumference (km)[c]	Crater Diameter as % of Parent Body Circumference	Approximate Maximum Extent of Ejecta[d] (km)	Approximate Maximum Extent of Basin-Related Features[e] (km)	Extent of Basin Influence Normalized To Crater Diameter[f]	References[g] (ejecta and basin structures)
Imbrium	Moon	1145	3475	10,917	10	1266	3435	1.1–3	a
Nectaris	Moon	860	3475	10,917	8	1360	1540	1.6–1.8	b, c
Orientale	Moon	930	3475	10,917	9	1680	1800	1.8–1.9	b, d
Caloris	Mercury	1500	4879	15,328	10	1850	–	1.2	e
Rembrandt	Mercury	716	4879	15,328	5	–	–		–
Valhalla	Callisto	525	4821	15,146	3	1165	1800	2.2–3.4	f
Asgard	Callisto	340	4821	15,146	2	740	1000	2.2–2.9	
Rheasilvia	Vesta	450	525	1649	27	550	–	1.2	g
Veneneia	Vesta	400	525	1649	24	–	–		g
Urvara	Ceres	170	940	2953	6	420	585	2.5–3.4	h
Yalode	Ceres	260	940	2953	9	540	730	2.1–2.8	h

[a] Sources: Moon-Wilhelms (1987); Callisto-Bender et al. (1997); Mercury, Vesta, and Ceres-Gazetteer of Planetary Nomenclature (2016).
[b] Sources: Moon, Mercury, and Callisto-National Space Science Data Coordinated Archive (2016); Vesta and Ceres-mean equatorial diameter from Russell et al. (2012, 2016).
[c] Parent Body Circumference $= \pi$ x diameter.
[d] Distances from approximate basin center; measured on geologic maps where available; Imbrium extent defined by Fra Mauro Fm; Nectaris extent defined by Descartes Fm; Orientale extent defined by Hevelius Fm; Caloris defined by Odin Fm.
[e] Distances from approximate basin center; measured on geologic maps where available; Does not include antipodal terrains; Imbrium extent from estimates in Haskin et al. (2003); Nectaris defined by Janssen Fm; Orientale extent from estimates in Meyer et al. (2016).
[f] If range given, low end is from ejecta and high end from basin structures.
[g] References: a. Housen et al. (1983), Haskin et al. (2003); b. Wilhelms et al. (1979); Wilhelms (1987); c. Wilhelms and McCauley (1971) d. Scott et al. (1977); Meyer et al. (2016); e. Guest and Greeley (1983); f. Bender et al. (1997); g. Yingst et al. (2014); h. this work, Buczkowski et al. (2016), (Mest et al., 2017).

sults present an explanation for why these basins on Ceres have a relatively greater extent of influence than those of some other bodies – the lower gravitation may allow for greater distance traveled due to the rotation of the parent body under airborne impact material. The greater relative extent for Urvara compared to Yalode can be interpreted to be a consequence of Urvara's younger age; Urvara ejecta is fresher and thus easier to unambiguously identify and map.

Our mapping demonstrates that Urvara and Yalode ejecta deposits extend to distances of more than two crater diameters from the centers of these basins, comparable to the extents associated with basins on other planets of similar size relative to their parent bodies. The currently mapped ejecta blankets and associations interpreted between distal structures and these impact basins are thus consistent with what would be expected. Such basins on other bodies are used as stratigraphic markers, anchoring epochs and periods in the geologic timescale (e.g., the Imbrium and Orientale basins serve as markers for the beginning and ending of the Early Imbrian Epoch respectively (Wilhelms, 1987 and references therein)). We suggest that the large areal extents of Urvara and Yalode's mapped ejecta blankets and the associated basin structures are important global stratigraphic markers that can be used for establishing the geologic timescale of Ceres. We also note that the similarity of ejecta extents for large impact structures on different Solar System bodies indicates that Ceres behaves in a grossly similar physical way to other small, airless, rocky bodies.

6. Geologic history

Our geologic mapping investigation of the Urvara and Yalode Quadrangles of Ceres utilizes Dawn FC datasets to identify, define, and map geologic units based on their morphology, topographic properties, and albedo and color characteristics. These observations also document stratigraphic and cross-cutting relationships that allow us to determine the relative ages of geologic units and processes and derive the geologic history of this region of Ceres. Because of the large size of the Urvara and Yalode basins and the great spatial extent of their associated deposits, the evolution of the region can be divided in a straightforward manner and summarized in several distinct steps. Observed contact relationships are documented in Table 2 and a synthesis of the geologic history is provided in Fig. 13.

The oldest geologic unit is the cratered terrain, which represents the ancient crust of Ceres that recorded a multitude of impact events over much of the dwarf planet's history. The Yalode basin formed in these ancient crustal materials and Yalode's ejecta was deposited on top of the cratered terrain surrounding the basin. Yalode's ejecta extends to the south into the Zadeni Quadrangle

Table 2
Urvara and Yalode Quadrangles: contact relationships between Units.

Unit	Contacts w/	Older than unit	Overlaps w/unit	Younger Than unit
crt	Ue, UYs, Ye, c, ccp, cfh, cfs		ccp	Ue, UYs, Ye, c, cfh, cfs
c	Ue, Ut, Ufh, UYs, Ye, Yfh, crt, ccp, ct, cfh, cfs	Ut, Ufh, UYs, Ye, Yfh, crt, ccp, cfs	Ue, UYs, ct	Ue, cfh
ccp	crt, c, ct, cfh, cfs		crt, c, ct	c, cfh, cfs
ct	c, ccp		c, ccp	
cfh	crt, c, ccp	crt, c, ccp		
cfs	crt, ccp	crt, ccp		
Ue	Ut, UYs, Ye, crt, c	Ye, crt	Ut, UYs, c	UYs, c
Ucp	Ufh, Ufs, UYs		UYs	UYs, Ufh, Ufs
Ut	Ue, Ufs, UYs, c		Ue, UYs	Ufs, UYs, c
Ufh	Ucp, Ufs, UYs, c	Ucp	UYs	Ufs, c
Ufs	Ut, Ufh, UYs	Ut, Ufh, UYs		
UYs	Ue, Ucp, Ut, Ufh, Ufs, Ye, Yfh, crt, c	Ue, Ucp, Ut, Ye, Yfh, crt	Ue, Ut, Ucp, Ufh,,c	Ufs, c
Ye	Ue, UYs, Yfh, crt, c	crt		Ue, UYs, Yfh, c
Yfh	UYs, Ye, c	Ye		UYs, c

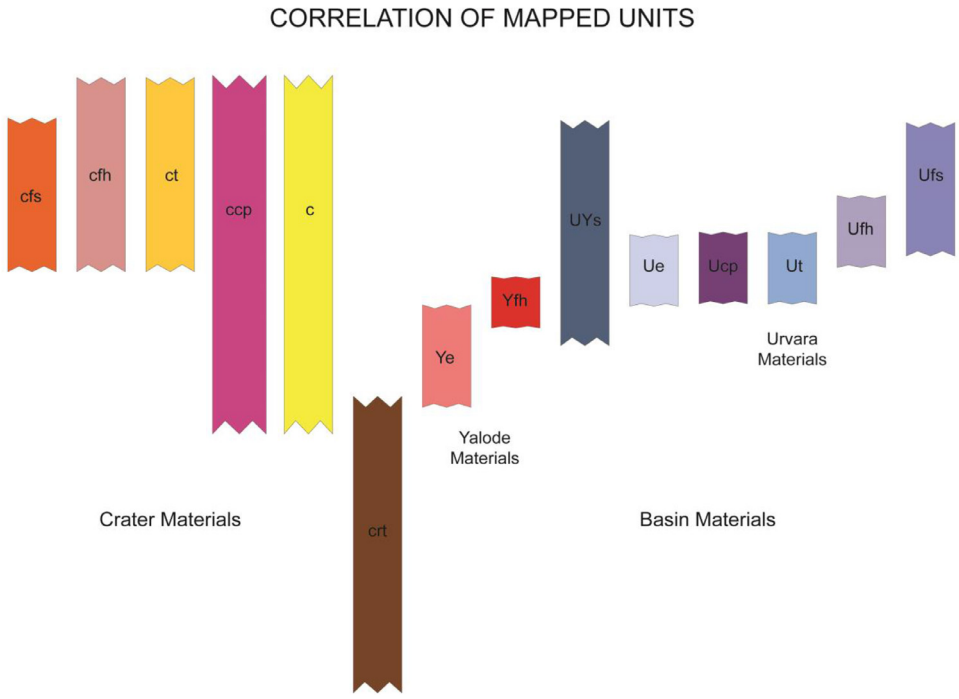

Fig. 13. Correlation of map units for geologic units in the Urvara and Yalode Quadrangles of Ceres based on observed stratigraphic relationships and geologic characteristics. (For interpretation of the references to color in this figure legend, the reader is referred to the web version of this article.)

and to the north into the Rongo Quadrangle, where secondary crater chains and fractures are also apparent. Yalode ejecta is not evident much beyond the basin's poorly-defined eastern rim; presumably the ejecta was originally less well developed here relative to other directions (perhaps due to Ceres' rotation) such that it has merged into the cratered terrain closer to the basin in this direction. Yalode's ejecta to the west is not apparent due to deposits associated with Urvara. The Urvara impact occurred after the Yalode impact, emplacing ejecta in all directions and covering the cratered terrain to the north, west, and south and Yalode basin to the east. Secondary crater chains that extend from Urvara's rim across the western margin of the Yalode basin and the morphologic differences between the basins clearly indicate this sequence of basin formation. Yalode and Urvara both exhibit interior units that occurred as part of or likely closely followed their impact events, including the development of terraces and a central peak in Urvara and hummocky floor deposits in both basins. The youngest regional unit is the Urvara/Yalode smooth material, which comprises much of floors of both basins but also extends to the north of Urvara and east of Yalode. Given the distribution of this unit, its lack of topographic control, and the fact that smooth material is superimposed on remnants of underlying basin rim materials, this unit is interpreted to be dominated by Urvara ejecta but also may contain Yalode ejecta and perhaps localized ice-rich mass-wasting and/or flow deposits. The Urvara floor material smooth unit covers a localized zone on the southern part of Urvara's floor and is among the youngest map units. Impact craters and their ejecta, rim, and floor deposits are mapped across the region. Differences in preservation state and relative age are inferred on the basis of the definition and character of ejecta margins. Some craters (e.g., 23°S, 279°E in NW Yalode and 54°S, 272°E in SW Yalode) show highly sinuous, distal ejecta margins and the presence of discrete ejecta lobes, as well as prominent talus deposits covering significant portions of their inner rims. These morphologic signatures indicate that the impacts forming these craters may be among the youngest geologic events in the region.

Crater populations in the Urvara and Yalode regions of Ceres have been examined for the purpose of deriving age estimates for geologic materials and events, including the formation of the Urvara and Yalode basins. The crater database compiled by Adrian Neesemann (May 31, 2016 version) was used to identify and extract crater diameters for the crater counting regions of interest. A small number of additional craters were added to the database given examination of the LAMO mosaic. Given uncertainties regarding the nature of the surface materials of Ceres that could be included in ejecta deposits and the apparent thin and diffuse nature of ejecta deposits around impact craters on Ceres, it is very difficult to assess whether small craters with less than pristine morphologies are degraded craters superposed on the surface of interest or craters that formed on the surface beneath and show through a thin ejecta blanket. Similar issues exist with large degraded craters but their stratigraphic position can be more reliably inferred. Effects of large craters that pre-date the unit of interest on model age estimates of the superposed unit can be mitigated by excluding specific craters from counts and/or restricting the fit range at the larger sizes. In any case, specific age determinations for geologic units on Ceres should be treated with caution as they depend to a significant degree on the population of craters identified and the fit range selected. Fit ranges are chosen based on visual inspection of which range of bins best match the shape of the production function on a differential plot. As understanding of the geology of Ceres progresses with continued analyses of Dawn mission datasets, age constraints will likely be improved.

Crater counting areas, craters included in crater counts, crater size-frequency distributions (CSFDs), and related statistics and results are shown in Fig. 14 and Table 3. The crater size-frequency distribution measurements are based on the LAMO mosaics and use of the CraterTools add-in to calculate crater diameters and counting areas (Kneissl et al., 2011). Crater plots conform to specifications in Crater Analysis Techniques Working Group (1979). Derived ages are shown in Table 3 for both the lunar-derived (LDM) and asteroid-derived (ADM) chronology systems (Hiesinger et al., 2016); the subsequent discussion uses the lunar-

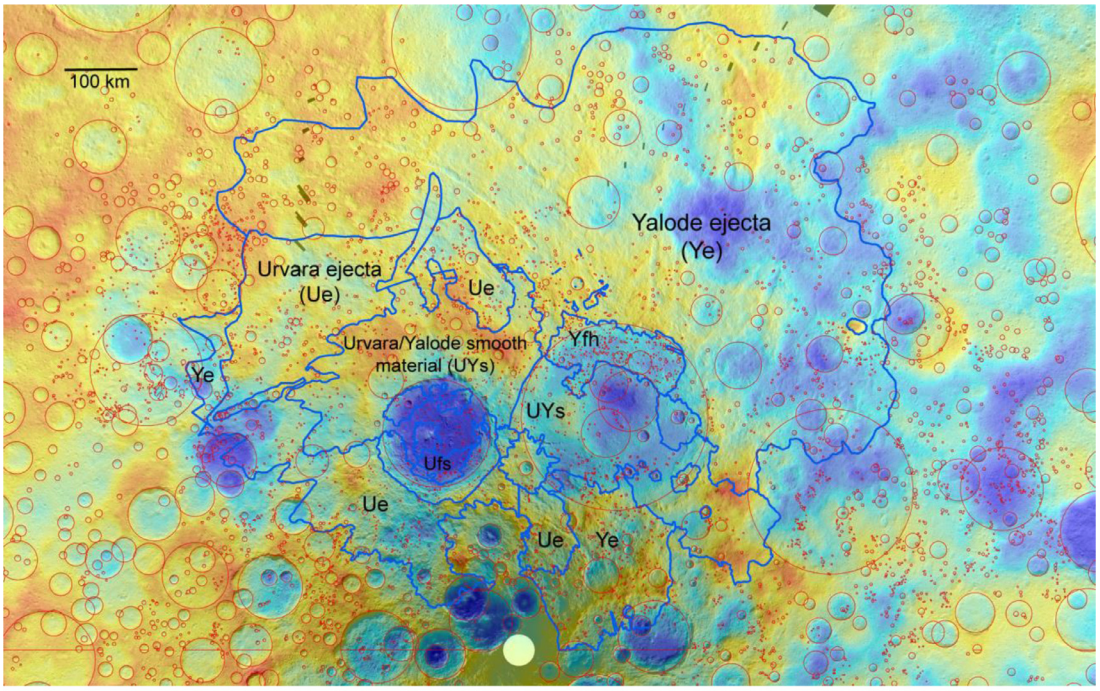

(a)

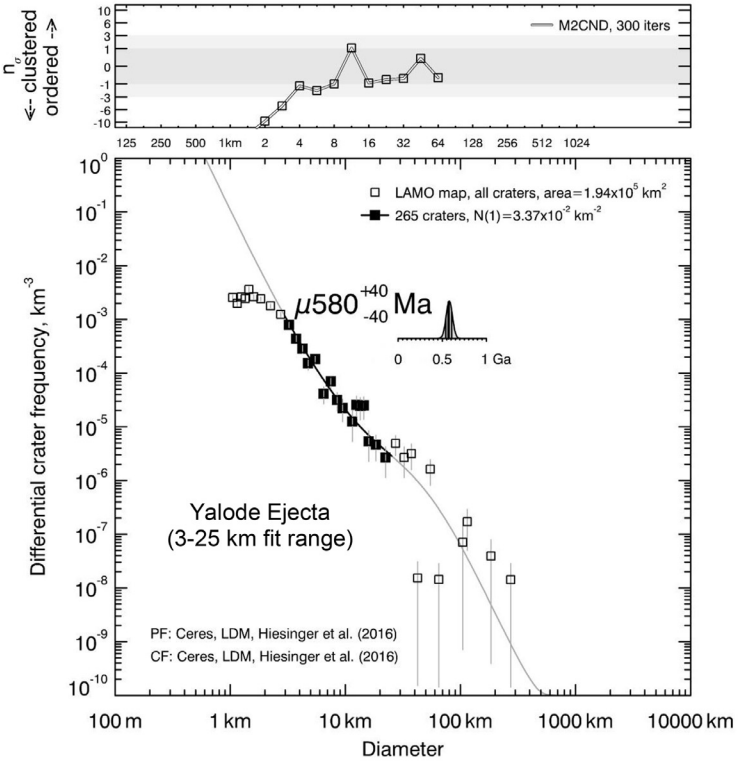

(b)

Fig. 14. Age estimates for the Urvara/Yalode region of Ceres. a) Crater counting areas within the Urvara and Yalode Quadrangles outlined in blue with crater rims shown in red. Craters from database of Adrian Neesemann (May 31, 2016 version), added to where additional craters recognized in LAMO mosaics. Crater counting areas labeled with unit names and/or abbreviations (Yfh = Yalode floor material hummocky and Ufs = Urvara floor material smooth). See text for discussion and Table 3 for crater statistics, including age estimates based on the lunar-derived (LDM) and asteroid-derived (ADM) models. Background is HAMO DTM merged with LAMO global mosaic in south polar stereographic projection with center longitude of 270°W. Yellow circle at bottom center corresponds to south pole data gap; b-f) Crater size-frequency distributions for areas in the Urvara/Yalode region, including Yalode ejecta material (b), Urvara ejecta material (c), Urvara/Yalode smooth material (d), Yalode floor material hummocky (e), and Urvara floor material smooth (f). Crater size-frequency distribution plots generated and model age estimates derived using CraterStats software (Michael and Neukum, 2010). The μ notation indicates that model ages have inherent uncertainties due to uncertainties in the production function; error bars represent statistical uncertainties in ages based on the production function. Results of randomness test are shown above each CSFD and Poisson uncertainty distributions are included next to model ages. (For interpretation of the references to color in this figure legend, the reader is referred to the web version of this article.)

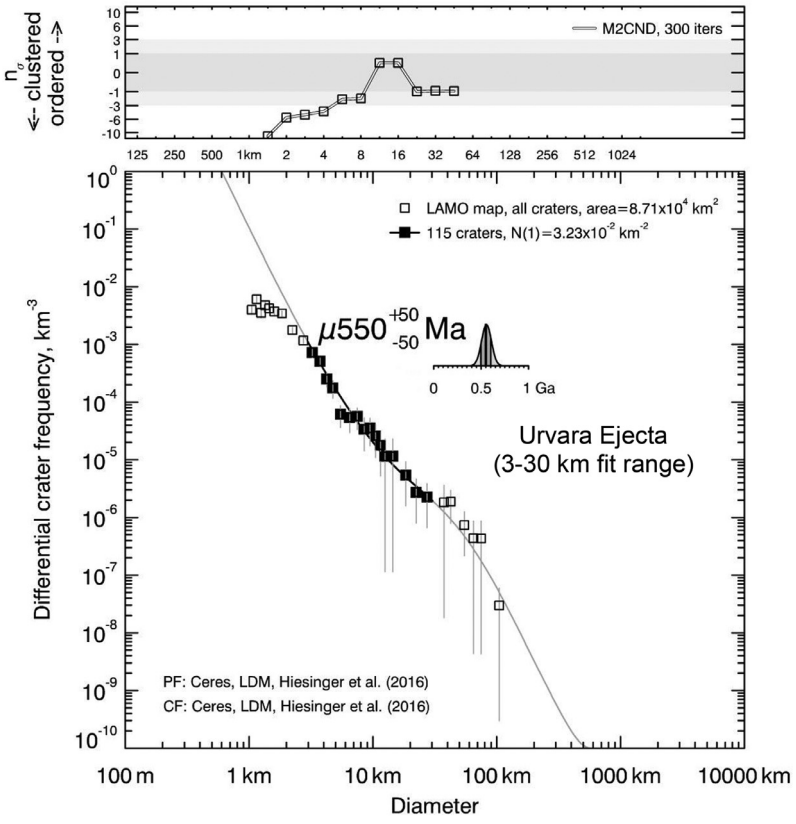

(c)

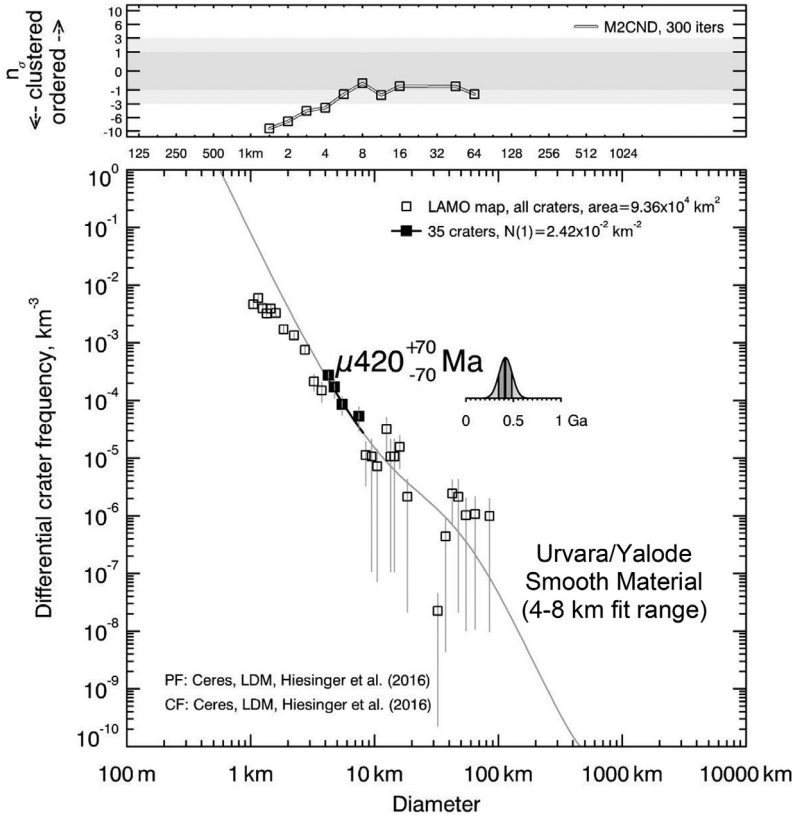

(d)

Fig. 14. Continued

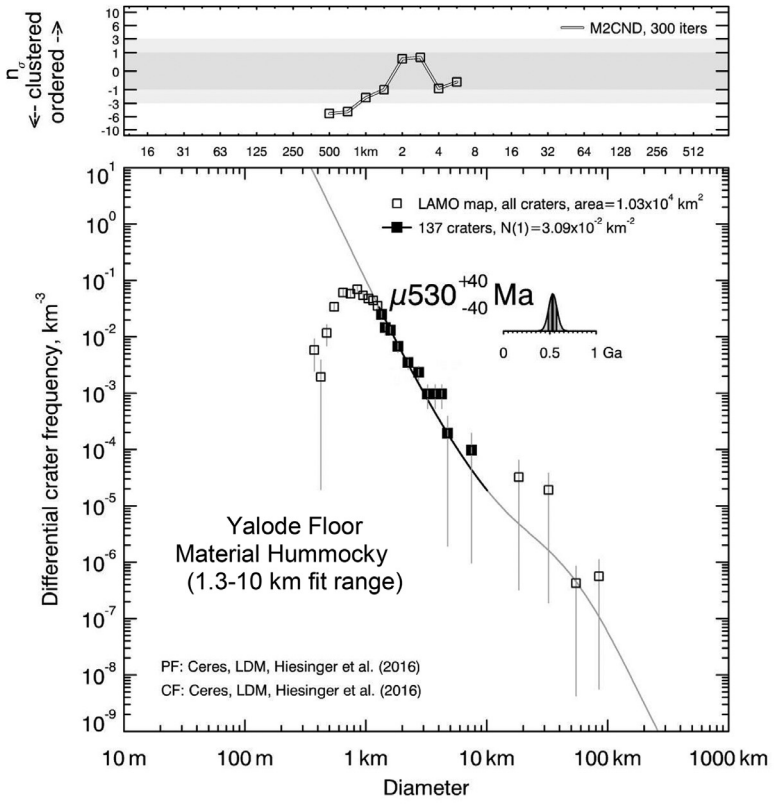

(e)

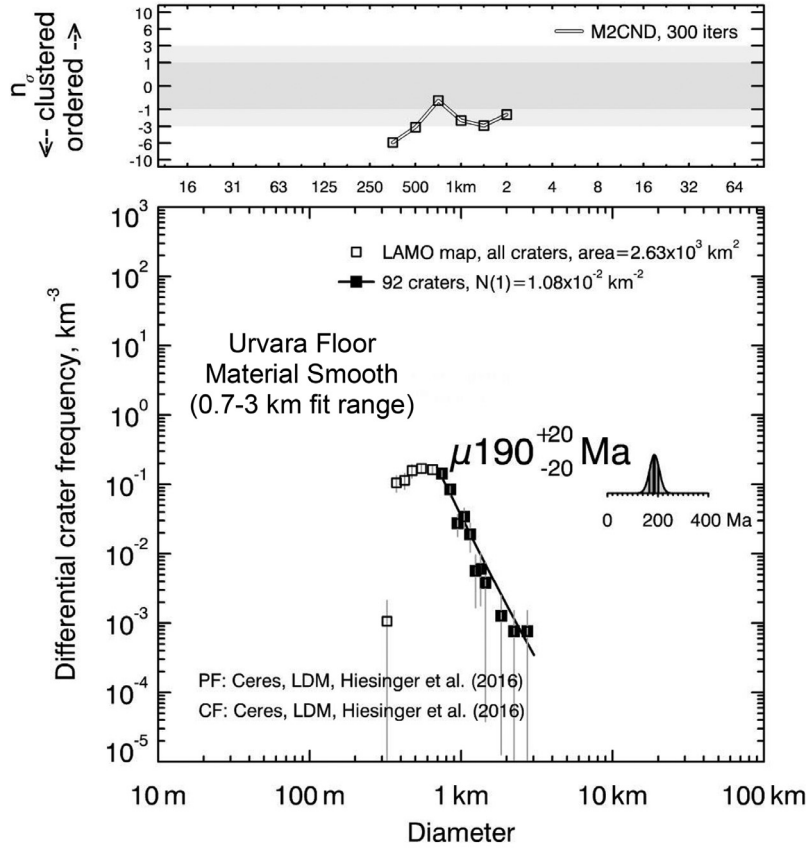

(f)

Fig. 14. Continued

Table 3
Crater counting parameters.

Crater Count Region	Area (km^2)	Total # Craters	Crater Size Range (km)	Fit Range (km)	# Craters in Fit Range	LDM[a] (Ma)	LDM Error (Ma)	ADM[b]	ADM Error (Ma)
Ye	194,385	1103	1–200	3–25	265	580	±40	120	±8
Ue	87,106	624	1–105	3–30	115	550	±50	120	±10
UYs	93,647	498	1–82	4–8	35	420	±70	86	±10
UYs (west)	45,796	291	1–47	4–8	19	480	±100	98	±20
UYs (east)	47,852	207	1–82	4–10	18	390	+100/−80	81	±20
Yfh	10,322	570	0.3–82	1.3–10	137	530	±40	140	±10
Ufs	2626	231	0.3–3	0.7–3	92	190	±20	73	±8

[a] Lunar-derived model age.
[b] Asteroid-derived model age.

derived ages. CraterStats software (Michael and Neukum, 2010; Michael et al., 2012; 2016) was used for plotting and fitting the crater size-frequency distributions, model age calculations, and statistical characterizations (including randomness analysis and Poisson uncertainty distributions).

We have compiled CSFDs and estimated model ages (LDM model included here) for the following units in the Urvara and Yalode Quadrangles: Yalode ejecta material (580 ± 40 Ma), Urvara ejecta material (550 ± 50 Ma), Urvara/Yalode smooth material (420 ± 70 Ma), Yalode floor material hummocky (530 ± 40 Ma), and Urvara floor material smooth (190 ± 20 Ma). The crater counting areas shown in Fig. 14 correspond to unit contacts mapped from LAMO mosaics for the Urvara (Fig. 3), Yalode (Fig. 3), Occator (Buczkowski et al., 2017), Rongo (Platz et al., 2017), and Zadeni (Williams et al., 2017a) Quadrangles (note: there are some slight discrepancies across quadrangle boundaries). In general, all model ages are consistent with the geologic history derived from mapping. The LDM absolute model ages for the basin ejecta materials are consistent with the distinct morphologic and stratigraphic information that indicates Yalode basin formed before Urvara basin. However, the absolute model ages are statistically inseparable and suggest that the impacts may have occurred relatively closely in geologic time. This is important given their spatial association and the inferred overlapping nature of both their ejecta deposits and floor materials (i.e., Urvara/Yalode smooth material) in terms of identifying useful stratigraphic markers for Ceres. Their close spatial and temporal associations mean they could be considered together as a single stratigraphic referent. The absolute model age for Urvara/Yalode smooth material is consistent with geologic analyses, in that the age is younger than the ages derived for both the Urvara and Yalode basins. Given our observations that Urvara/Yalode smooth material appears to extend across both basin floors and parts of both basin rims, we tested our interpretation of this unit as containing deposits from both basins by examining CSFDs of the western (Urvara) and eastern (Yalode) parts (Fig. 14). Table 3 shows a slightly older model age for the western part versus the eastern part (480 ± 100 Ma vs. 390 + 100/−80 Ma) but the ages overlap. This supports our statements regarding the lack of clear contacts between the floor materials of the two basins. The absolute model age estimated for Yalode floor material hummocky overlaps with but is slightly younger than the age for Yalode ejecta, consistent with our interpretation of this unit as degraded terrace materials along Yalode's northern rim. The absolute model age for Urvara floor material smooth is much younger than for other geologic units in the region, consistent with its smooth and lightly cratered appearance. This age supports hypotheses regarding remobilization of ice-rich floor materials and/or localized cryovolcanism on the Urvara basin floor.

7. Conclusions

Geologic mapping of the 1:500,000-scale Urvara (Ac-13; 21–66°S, 180–270°E) and Yalode (Ac-14; 21–66°S, 270–360°E) Quadrangles of Ceres has shown the following:

(1) Cratering dominated the geologic history of the Urvara and Yalode Quadrangles; impact craters display a wide range in preservation states from nearly completely degraded/buried to pristine, and resurfacing across the map region appears to have been predominantly impact-related;
(2) The geologic history of the map region included early formation of cratered terrain, a middle phase of basin formation, and late-stage emplacement of smooth deposits and impact events from continued cratering;
(3) On the basis of cross-cutting relationships and morphologic signatures, the formation of Urvara basin post-dates the formation of Yalode basin;
(4) Widespread smooth deposits are associated with Urvara and Yalode and extend across variable topography and elevations; they are interpreted to be dominated by Urvara ejecta but may also include Yalode ejecta. Localized ice-rich extrusive material cannot be ruled out and may play a minor role.
(5) Comparisons between Urvara, Yalode and other basins in the region indicate variable degradational sequences for impact craters, some of which show prominent terrace formation. Terraced inner crater walls may degrade into hummocky floor material, facilitate localized ice-rich mass wasting, and with continued modification exhibit smooth surfaces;
(6) Heterogeneities in Urvara basin materials and morphologic variability along the rims of both basins may result from heterogeneities in the substrate encountered during impact, with smooth deposits containing greater proportions of ice and steep scarps reflecting relatively stronger crustal materials;
(7) Ejecta simulations and comparisons with other planetary bodies are consistent with mapping results that suggest Urvara and Yalode ejecta deposits extend for large distances and may serve as important stratigraphic markers for the geologic record of Ceres; and
(8) Crater size-frequency distributions for geologic units within the Urvara and Yalode Quadrangles (and extending into surrounding regions) support relative age interpretations based on geologic mapping and provide absolute age estimates (using the lunar-derived model (see Hiesinger et al., 2016)) for the formation of the Yalode basin (580 ± 40 Ma), the Urvara basin (550 ± 50 Ma), the Urvara/Yalode smooth material (420 ± 70 Ma), Yalode floor material hummocky (530 ± 40 Ma), and Urvara floor material smooth (190 ± 20 Ma).

Acknowledgements

This research has been enabled by the many individuals involved in the successful operations of the Dawn Mission at Ceres, including the NASA Dawn Science and Flights teams at the Jet Propulsion Laboratory and the instrument teams at the Max Planck Institute for Solar System Research, the German Aerospace Center (DLR), the Italian National Institute for Astrophysics (INAF), and the Planetary Science Institute (PSI). We thank two anonymous reviewers for their comments that improved the presentation of this research. We acknowledge support from the NASA Dawn at

Ceres Guest Investigator Program (NNX15AI36G). We thank Andrea Nass (DLR) for creating the template for quadrangle mapping of Ceres and importing the Urvara and Yalode maps into it and Adrian Neesemann for providing his crater catalogue (May 31, 2016 version) to facilitate our derivation of age estimates for geologic units.

Supplementary materials

Supplementary material associated with this article can be found, in the online version, at doi:10.1016/j.icarus.2017.08.004.

References

Ammannito, E., De Sanctis, M.C., Ciarniello, M., Frigeri, A., Carrozzo, F.G., Combe, J.-Ph., Ehlmann, B.L., Marchi, S., McSween, H.Y., Raponi, A., Toplis, M., Tosi, F., Castillo-Rogez, J.C., Capaccioni, F., Capria, M.T., Fonte, S., Giardino, M., Jaumann, R., Longobardo, A., Joy, S.P., Magni, G., McCord, T.B., McFadden, L.A., Palomba, E., Pieters, C.M., Polanskey, C.A., Rayman, M.D., Raymond, C.A., Schenk, P., Zambon, F., Russell, C.T.the Dawn Science Team, 2016. Distribution of phyllosilicates on Ceres. Science 353. doi:10.1126/science.aaf4279.

Bender, K.C., Rice, J.W., Wilhelms, D.E., Greeley, R., 1997. Geologic map of Callisto. U.S. Geol. Surv. Misc. Inv. Series Map I-2581.

Bierhaus, E.B., Dones, L., Alvarellos, J.L., Zahnle, K., 2012. The role of ejecta in the small crater populations on the mid-sized saturnian satellites. Icarus 218, 602–621.

Bland, M.T., Raymond, C.A., Schenk, P.M., Fu, R.R., Kneissl, T., Pasckert, J.H., Hiesinger, H., Preusker, F., Park, R.S., Marchi, S., King, S.D., Castillo-Rogez, J.C., Russell, C.T., 2016. Composition and structure of the shallow subsurface of Ceres revealed by crater morphology. Nature Geosci. 9, 538–543.

Buczkowski, D.L., Schmidt, B., Williams, D.A., Mest, S.C., Scully, J.E.C., Ermakov, A.I., Preusker, F., Schenk, P., Otto, K.A., Hiesinger, H., O'Brien, D., Marchi, S., Sizemore, H., Hughson, K., Chilton, H., Bland, M., Byrne, S., Schorghofer, N., Platz, T., Jaumann, R., Roatsch, T., Sykes, M.V., Nathues, A., De Sanctis, M.C., Raymond, C.A., Russell, C.T., 2016. The geomorphology of Ceres. Science 353. doi:10.1126/science.aaf4332.

Buczkowski, D.L., Williams D.A., Scully J.E.C., Mest S.C., Crown D.A., Schenk P.M., Jaumann R., Roatsch T., Preusker F., Platz T., Nathues A., Hoffman M., Schaefer M., Marchi S., De Sanctis M.C., Raymond C.A., Russell C.T., 2017. The geology of the Occator Quadrangle of dwarf planet Ceres: floor-fractured craters and other geomorphic evidence of cryomagmatism. Icarus, accepted for publication, this issue.

Castillo-Rogez, J.C., McCord, T.B., 2010. Ceres' evolution and present state constrained by shape data. Icarus 205, 443–459. doi:10.1016/j.icarus.2009.04.008.

Combe, J-P., McCord, T.B., Tosi, F., Ammannito, E., Carrozzo, F.G., De Sanctis, M.C., Raponi, A., Byrne, S., Landis, M.E., Hughson, K.H.G., Raymond, C.A., Russell, C.T., 2016. Detection of local H_2O exposed at the surface of Ceres. Science 353. doi:10.1126/science.aaf3010.

Crater Analysis Techniques Working Group, 1979. Standard techniques for presentation and analysis of crater size-frequency data. Icarus 37, 467–474.

Crown, D.A., Yingst, R.A., Mest, S.C., Platz, T., Williams, D.A., Buczkowski, D.L., Schenk, P.M., Scully, J.E.C., Jaumann, R., Roatsch, T., Preusker, F., Nathues, A., Hoffman, M., Schaeffer, M., Marchi, S., De Sanctis, M.C., Russell, C.T., Raymond, C.A., 2015. Preliminary geological map of the Ac-H-14 Yalode Quadrangle of Ceres: an integrated mapping study using Dawn spacecraft data. Abstract P53E-2181, 2015 Fall Meeting, AGU, San Francisco, Calif., 14-18 Dec.

Crown, D.A., Yingst, R.A., Mest, S.C., Platz, T., Sizemore, H.G., Berman, D.C., Williams, D.A., Roatsch, T., Preusker, F., Nathues, A., Hoffman, M., Schäfer, M., Raymond, C.A., Russell, C.Tthe Dawn Science Team, 2016a. Geologic mapping of the Ac-H-14 Yalode Quadrangle of Ceres from NASA's Dawn Mission. Lunar and Planetary Science Conference XLVII, Abstract 1602, Lunar and Planetary Institute, Houston.

Crown, D.A., Yingst, R.A., Mest, S.C., Platz, T., Sizemore, H.G., Berman, D.C., Williams, D.A., Roatsch, T., Preusker, F., Nathues, A., Hoffman, M., Schäfer, M., Raymond, C.A., Russell, C.Tthe Dawn Science Team, 2016b. Geological mapping of the Ac-H-14 Yalode Quadrangle of Ceres from NASA's Dawn Mission. Abstract EGU2016-9445, EGU General Assembly, Vienna, Austria, 17-22 April.

Denevi, B.W., Blewett, D.T., Buczkowski, D.L., Capaccioni, F., Capria, M.T., De Sanctis, M.C., Garry, W.B., Gaskell, R.W., Le Corre, L., Li, J.-Y., Marchi, S., McCoy, T.J., Nathues, A., O'Brien, D.P., Petro, N.E., Pieters, C.M., Preusker, F., Raymond, C.A., Reddy, V., Russell, C.T., Schenk, P., Scully, J.E.C., Sunshine, J.M., Tosi, F., Williams, D.A., Wyrick, D., 2012. Pitted terrain on Vesta and implications for the presence of volatiles. Science 338, 246–249.

De Sanctis, M.C., Ammannito, E., Raponi, A., Marchi, S., McCord, T.B., McSween, H.Y., Capaccioni, F., Capria, M.T., Carrozzo, F.G., Ciarniello, M., Longobardo, A., Tosi, F., Fonte, S., Formisano, M., Frigeri, A., Giardino, M., Magni, G., Palomba, E., Turrini, D., Zambon, F., Combe, J.-P., Feldman, W., Jaumann, R., McFadden, L.A., Pieters, C.M., Prettyman, T., Toplis, M., Raymond, C.A., Russell, C.T., 2016. Ammoniated phyllosilicates with an outer solar system origin on (1) Ceres. Nature 528, 241–244.

Gazetteer of Planetary Nomenclature, 2106. http://planetarynames.wr.usgs.gov.

Guest, J.E., Greeley, R., 1983. Geologic map of the Shakespeare Quadrangle of Mercury. U.S. Geol. Surv. Misc. Inv. Series Map I-1408.

Haskin, L.A., Moss, B.E., McKinnon, W., 2003. On estimating ejecta deposit thicknesses and proportions of materials from distant basins at lunar highland sites. Met. Planet. Sci. 38, 13–33.

Hiesinger, H., Marchi, S., Schmedemann, N., Schenk, P., Pasckert, J.H., Neesemann, A., O'Brien, D.P., Kneissl, T., Ermakov, A.I., Fu, R.R., Bland, M.T., Nathues, A., Platz, T., Williams, D.A., Jaumann, R., Castillo-Rogez, J.C., Ruesch, O., Schmidt, B., Park, R.S., Preusker, F., Buczkowski, D.L., Russell, C.T., Raymond, C.A., 2016. Cratering on Ceres: implications for its crust and evolution. Science 353. doi:10.1126/science.aaf4759.

Housen, K.R., Schmidt, R.M., Holsapple, K.A., 1983. Crater ejecta scaling laws: fundamental forms based on dimensional analysis. J. Geophys. Res. 88, 2485–2499 doi:10/1029/JB088iB03p02485.

Kneissl, T., van Gasselt, S., Neukum, G., 2011. Map-projection-independent crater size-frequency determination in GIS environments—New software tool for ArcGIS. Planet. Space Sci. 59, 1243–1254.

Küppers, M., O'Rourke, L., Bockelee-Morvan, D., Zakharov, V., Lee, S., von Allmen, P., Carry, B., Teyssier, D., Marston, A., Müller, T., Crovisier, J., Barucci, M.A., Moreno, R., 2014. Localized sources of water vapour on the dwarf planet (1) Ceres. Nature 505, 525–527.

Lebofsky, L.A., Feierberg, M.A., Tokunaga, A.T., Larson, H.P., Johnson, J.R., 1981. The 1.7- to 4.2-um spectrum of asteroid 1 Ceres: evidence for structural water in clay minerals. Icarus 48, 453–459. doi:10.1016/0019-1035(81)90055-5.

Lebofsky, L.A., Sykes, M.V., Tedesco, E.F., Veeder, G.J., Matson, D.L., Brown, R.H., Gradie, J.C., Feierberg, M.A., Rudy, R.J., 1986. A refined 'standard' thermal model for asteroids based on observations of 1 Ceres and 2 Pallas. Icarus 68, 239–251.

Marchi, S., Ermakov, A.I., Raymond, C.A., Fu, R.R., O'Brien, D.P., Bland, M.T., Ammannito, E., De Sanctis, M.C., Bowling, T., Schenk, P., Scully, J.E.C., Buczkowski, D.L., Williams, D.A., Hiesinger, H., Russell, C.T., 2016. The missing large impact craters on Ceres. Nat. Comm. doi:10.1038/ncomms12257.

McCord, T.B., Sotin, C., 2005. Ceres: evolution and current state. J. Geophys. Res. 110, E05009. doi:10.1029/2004JE002244.

Melosh, H.J., 1996. Impact Cratering: A Geologic Process. Oxford University Press, p. 245.

Mest, S.C., Crown, D.A., Yingst, R.A., Berman, D.C., Williams, D.A., Buczkowski, D.L., Scully, J.E.C., Platz, T., Jaumann, R., Roatsch, T., Preusker, F., Nathues, A., Raymond, C.A., Russell, C.T., 2016. Update on the global geologic map of Ceres from NASA's Dawn mission, Geol. Soc. Amer. Abstracts with Program 48 (7) Abstract 285745.

Mest, S.C. et al., 2017. Global geologic mapping of Ceres. Icarus, in preparation, this issue.

Meyer, H.M., Denevi, B.W., Boyd, A.K., Robinson, M.S., 2016. The distribution and origin of lunar light plains around Orientale basin. Icarus 273, 135–145. doi:10.1016/j.icarus.2016.02.014.

Michael, G.G., Neukum, G., 2010. Planetary surface dating from crater size-frequency distribution measurements: partial resurfacing events and statistical age uncertainty. Earth Planet. Sci. Lett. 294, 223–229.

Michael, G.G., Platz, T., Kneissl, T., Schmedemann, N., 2012. Planetary surface dating from crater size-frequency distribution measurements: spatial randomness and clustering. Icarus 218, 169–177.

Michael, G.G., Kneissl, T., Neeseman, A., 2016. Planetary surface dating from crater size-frequency distribution measurements: Poisson timing analysis. Icarus 277, 279–285.

Milliken, R.E., Rivkin, A.S., 2009. Brucite and cardonate assemblages from altered olivine-rich materials on Ceres. Nat. Geosci. 2, 258–261. doi:10.1038/ngeo478.

Nass, A., 2017. One GIS-based data structure for geological mapping using 15 map sheets—Dawn at Ceres. 48th Lunar and Planetary Science Conference, abstract 1892.

National Space Science Data Coordinated Archive, 2016. http://nssdc.gsfc.nasa.gov.

Nathues, A., Hoffmann, M., Cloutis, E.A., Schäfer, M., Reddy, V., Christensen, U., Sierks, H., Thangjam, G.S., Le Corre, L., Mengel, K., Vincent, J.-B., Russell, C.T., Prettyman, T., Schmedemann, N., Kneissl, T., Raymond, C., Gutierrez-Marques, P., Hall, I., Büttner, I., 2014. Detection of serpentine in exogenic carbonaceous chondrite material on Vesta from Dawn FC data. Icarus 239, 222–237.

Nathues, A., Hoffmann, M., Schaefer, M., Le Corre, L., Reddy, V., Platz, T., Cloutis, E.A., Christensen, U., Kneissl, T., Li, J.-Y., Mengel, K., Schmedemann, N., Schaefer, T., Russell, C.T., Applin, D.M., Buczkowski, D.L., Izawa, M.R.M., Keller, H.U., O'Brien, D.P., Pieters, C.M., Raymond, C.A., Ripken, J., Schenk, P.M., Schmidt, B.E., Sierks, H., Sykes, M.V., Thangjam, G.S., Vincent, J.-B., 2015. Sublimation in bright spots on (1) Ceres. Nature 528, 237–240. doi:10.1038/nature15754.

Nathues, A., Platz, T., Thangjam, G., Hoffman, M., Mengel, K., Cloutis, E.A., Le Corre, L., Reddy, V., Kallisch, J., Crown, D.A., 2017. Evolution of Occator crater on (1) Ceres. Astron. J. 153 doi:10.3847/1538-3881/153/3/112.

Park, R.S., Konopliv, A.S., Bills, B.G., Rambaux, N., Castillo-Rogez, J.C., Raymond, C.A., Vaughan, A.T., Ermakov, A.I., Zuber, M.T., Fu, R.R., Toplis, M.J., Russell, C.T., Nathues, A., Preusker, F., 2016. A partially differentiated interior for (1) Ceres deduced from its gravity field and shape. Nature 537, 515–517. doi:10.1038/nature18955.

Petro, N.E., Pieters, C.M., 2008. The lunar-wide effects of basin ejecta distribution on the early megaregolith. Met. Planet. Sci. 43, 1517–1529.

Platz, T., Nathues, A., Schorghofer, N., Preusker, F., Mazarico, E., Schröder, S.E., Byrne, S., Kneissl, T., Schmedemann, N., Combe, J.-Ph., Schäfer, M., Thangjam, G.S., Hoffmann, M., Gutierrez-Marques, P., Landis, M.E., Dietrich, W., Ripken, J., Matz, K.-D., Russell, C.T., 2016a. Surface water ice deposits in the northern shadowed regions of Ceres. Nature Astron. 1, 0007. doi:10.1038/s41550-016-0007.

Platz, T., Nathues, A., Sizemore, H.G., Ruesch, O., Hoffman, M., Schaefer, M., Crown, D.A., Mest, S.C., Yingst, R.A., Williams, D.A., Buczkowski, D.L., Hughson, K., Kneissl, T., Schmedemann, N., Schorghofer, N., Naß, A., Preusker, F., Russell, C.T., 2016b. Geological mapping of the Ac-H-10 Rongo and Ac-H-15 Zadeni quadrangles of Ceres from NASA's Dawn mission. Abstract EGU2016-18352, EGU General Assembly, Vienna, Austria, 17-22 April.

Platz, T., Nathues, A., Ruesch, O., Sizemore, H.G., Schaefer, M., Hoffman, M., Crown, D.A., Mest, S.C., Yingst, R.A., Williams, D.A., Kneissl, T., Schmedemann, N., Naß, A., Preusker, F., 2016c. Geologic mapping of the Ac-H-10 Rongo quadrangle of Ceres. abstract 7030, Abstracts of the Annual Meeting of Planetary Geologic Mappers, Flagstaff, AZ, 2016.

Platz, T., Nathues A., Sizemore H.G., Crown D.A., Hoffman M., Schäfer M., Schmedemann N., Kneissl T., Neeseman A., Mest S.C., Buczkowski D.L., Ruesch O., Hughson K.H.G., Naß A., Williams D.A., Preusker F., 2017. Geologic mapping of the Ac-10 Rongo Quadrangle of Ceres. Icarus, in review, this issue.

Prettyman, T.H., Yamashita, N., Castillo-Rogez, J.C., Feldman, W.C., Lawrence, D.J., McSween, H.Y., Schorghofer, N., Toplis, M.J., Forni, O., Joy, S.P., Marchi, S., Platz, T., Polansky, C.A., De Sanctis, M.C., Rayman, M.D., Raymond, C.A., Russell, C.T., 2016. Elementary composition of Ceres by Dawn's gamma ray and neutron detector. Lunar and Planetary Science Conference XLVII, Abstract 2228, Lunar and Planetary Institute, Houston.

Preusker, F., Scholten, F., Matz, K.-D., Elgner, S., Jaumann, R., Roatsch, T., Joy, S.P., Polanskey, C.A., Raymond, C.A., Russell, C.T., 2016. Dawn at Ceres-shape model and rotational state. Lunar and Planetary Science Conference XLVII, Abstract 1954, Lunar and Planetary Institute, Houston.

Reddy, V., Nathues, A., Le Corre, L., Sierks, H., Li, J.-Y., Gaskell, R., McCoy, T., Beck, A.W., Schröder, S.E., Pieters, C.M., Becker, K.J., Buratti, B.J., Denevi, B., Blewett, D.T., Christensen, U., Gaffey, M.J., Gutierrez-marques, P., Hicks, M., Keller, H.U., Maue, T., Mottola, S., McFadden, L.A., McSween, H.Y., Mittlefehldt, D., O'Brien, D.P., Raymond, C.A., Russell, C.T., 2012. Color and albedo heterogeneity of Vesta from Dawn. Science 336. doi:10.1126/science.1219088.

Rivkin, A.S., Volquardsen, E.L., Clark, B.E., 2006. The composition of Ceres: discovery of carbonates and iron-rich clays. Icarus 185, 563–567. doi:10.1016/j.icarus.2006.08.022.

Roatsch, T., Kersten, E., Matz, K.-D., Preusker, F., Scholten, F., Jaumann, R., Raymond, C.A., Russell, C.T., 2016. High-resolution Ceres high altitude mapping orbit atlas derived from Dawn framing camera images. Planet. Space Sci. 129, 103–107.

Roatsch, T., Kersten, E., Matz, K.-D., Preusker, F., Scholten, F., Jaumann, R., Raymond, C.A., Russell, C.T., 2017. High-resolution Ceres low altitude mapping Orbit atlas derived from Dawn framing camera images. Planet. Space Sci. 140, 74–79.

Ruesch, O., Platz, T., Schenk, P., McFadden, L.A., Castillo-Rogez, J.C., Quick, L.C., Byrne, S., Preusker, F., O'Brien, D.P., Schmedemann, N., Williams, D.A., Li, J.-Y, Bland, M.T., Hiesinger, H., Kneissl, T., Neesemann, A., Schaefer, M., Pasckert, J.H., Schmidt, B.E., Buczkowski, D.L., Sykes, M.V., Nathues, A., Roatsch, T., Hoffmann, M., Raymond, C.A., Russell, C.T., 2016. Cryovolcanism on Ceres. Science 353. doi:10.1126/science.aaf4286.

Russell, C.T., Raymond, C.A., 2011. The Dawn mission to Vesta and Ceres. Space Sci. Rev. 163, 3–23. doi:10.1007/s11214-011-9836-2.

Russell, C.T., et al., 2012. Dawn at Vesta: testing the protoplanetary paradigm. Science 336, 684–686. doi:10.1126/science.1219381.

Russell, C.T., et al., 2016. Dawn arrives at Ceres: exploration of a small, volatile-rich world. Science 353, 1008–1010. doi:10.1126/science.aaf4219.

Schorghofer, N., Mazarico, E., Platz, T., Preusker, F., Schroder, S., Raymond, C.A., Russell, C.T., 2016. The permanently shadowed regions of dwarf planet Ceres. Geophys. Res. Lett. 43. doi:10.1002/2016GL069368.

Scott, D.H., McCauley, J.F., West, M.N., 1977. Geologic map of the west side of the Moon. U.S. Geol. Surv. Misc. Inv. Ser. Map I-1034.

Scully, J.E.C., Raymond, C.A., Buczkowski, D.L., O'Brien, D.P., Mitri, G., King, S.D., Russell, C.T., Platz, T., 2016a. Implications for the geologic evolution of Ceres, derived from geologic mapping of linear features. Lunar and Planetary Science Conference XLVII, Abstract 1903, Lunar and Planetary Institute, Houston.

Scully, J.E.C., Buczkowski, D.L., King, S.D., Castillo, J.C., Schmedemann, N., Raymond, C.A., O'Brien, D.P., Marchi, S., Russell, C.T., Mitri, G., Bland, M.T., 2016b. The surface and interior evolution of Ceres revealed by analysis of fractures and secondary crater chains using Dawn data. Abstract P54A-05, 2016 Fall Meeting, AGU, San Francisco, Calif., 12-16 Dec.

Sierks, H., Keller, H.U., Jaumann, R., Michalik, H., Behnke, T., Bubenhagen, F., Büttner, I., Carsenty, U., Christensen, U., Enge, R., Fiethe, B., Gutierrez Marques, P., Hartwig, H., Kühne, H., Maue, T., Mottola, S., Nathues, A., Reiche, K.-U., Richards, M.L., Roatsch, T., Schröder, S.E., Szemerey, I., Tschentscher, M., 2011. The Dawn framing camera. Space Sci. Rev. 163, 263–327.

Sizemore, H.G., Williams, D.A., Platz, T., O'Brien, D.P., Mest, S.C., Crown, D.A., Yingst, R.A., Buczkowski, D.L., Schenk, P.M., Scully, J.E.C., 2015a. Initial geologic mapping of the AC-H-13 Urvara Quadrangle of Ceres using Dawn spacecraft data. Geol. Soc. Am. Abstracts with Program 47 (7) Abstract 308-13.

Sizemore, H.G., Williams, D.A., Platz, T., O'Brien, D.P., Mest, S.C., Yingst, R.A., Crown, D.A., Buczkowski, D.L., Schenk, P.M., Scully, J.E.C., Jaumann, R., Roatsch, T., Preusker, F., Nathues, A., De Sanctis, M.C., Russell, C.T., Raymond, C.A., 2015b. Preliminary geological map of the Ac-H-13 Urvara Quadrangle of Ceres: an integrated mapping study using Dawn spacecraft data. Abstract P53E-2180, 2015 Fall Meeting, AGU, San Francisco, Calif., 14-18 Dec.

Sizemore, H.G., Williams, D.A., Platz, T., Mest, S.C., Yingst, R.A., Crown, D.A., O'Brien, D.P., Buczkowski, D.L., Schenk, P.M., Scully, J.E.C., Jaumann, R., Roatsch, T., Preusker, F., Nathues, A., De Sanctis, M.C., Russell, C.T., Raymond, C.A., 2016a. Geologic mapping of the Ac-H-13 Urvara Quadrangle of Ceres from NASA's Dawn Mission. Lunar and Planetary Science Conference XLVII, Abstract 1599, Lunar and Planetary Institute, Houston.

Sizemore, H.G., Williams, D.A., Platz, T., Mest, S.C., Yingst, R.A., Crown, D.A., O'Brien, D.P., Buczkowski, D.L., Schenk, P.M., Scully, J.E.C., Jaumann, R., Roatsch, T., Preusker, F., Nathues, A., De Sanctis, M.C., Russell, C.T., Raymond, C.A., 2016b. Geological mapping of the Ac-H-13 Urvara Quadrangle of Ceres from NASA's Dawn Mission. Abstract EGU2016-10525, EGU General Assembly, Vienna, Austria, 17-22 April.

Sizemore, H.G., Platz, T., Schorghofer, N., Prettyman, T.H., De Sanctis, M.C., Crown, D.A., Schmedemann, N., Neesemann, A., Kneissl, T., Marchi, S., Schenk, P.M., Bland, M.T., Schmidt, B.E., Hughson, K., Tosi, F., Zambon, F., Mest, S.C., Yingst, R.A., Williams, D.A., Russell, C.T., Raymond, C.A., 2017. Pitted terrains on (1) Ceres and implications for shallow subsurface volatile distribution. Geophys. Res. Lett. 2017.

Thomas, P.C., et al., 2005. Differentiation of the asteroid Ceres as revealed by its shape. Nature 437, 224–226. doi:10.1038/nature03938.

Tornabene, L.L., Osinski, G.R., McEwen, A.S., Boyce, J.M., Bray, V.J., Caudill, C.M., Grant, J.A., Hamilton, C.W., Mattson, S., Mouginis-Mark, P.J., 2012. Widespread crater-related pitted materials on Mars: further evidence for the role of target volatiles during the impact process. Icarus 220, 348–368.

Wilhelms, D.E., 1987. The Geologic History of the Moon. U.S. Geol. Surv. Prof. Pap. 1348.

Wilhelms, D.E., McCauley, J.F., 1971. Geologic map of the near side of the Moon. U.S. Geol. Surv. Geol. Inv. Series Map I-703.

Wilhelms, D.E., Howard, K.A., Wilshire, H.G., 1979. Geologic map of the south side of the Moon. U.S. Geol. Surv. Misc. Inv. Series Map I-1162.

Williams, D.A., Buczkowski, D.L., Mest, S.C., Scully, J.E.C., Platz, T., and Kneissl, T. 2017a. Introduction: the geologic mapping of Ceres. Icarus, in press, this issue (https://doi.org/10.1016/j.icarus.2017.05.004).

Williams, D.A., Kneissl T., Neesemann A., Mest S.C., Palomba E., Platz T., Nathues A., Longobardo A., Scully J.E.C., Ermakov A., Jaumann R., Buczkowski D.L., Schäfer M., Thangjam G., Pieters C.M., Roatsch T., Preusker F., Marchi S., Schmedemann N., Hiesinger H., Frigeri A., Raymond C.A., Russell C.T., 2017b. The geology of the Kerwan Quadrangle of dwarf planet Ceres: investigating Ceres' oldest impact basin. Icarus, in review, this issue.

Yingst, R.A., Mest, S.C., Berman, D.C., Garry, W.B., Williams, D.A., Buczkowski, D., Jaumann, R., Pieters, C.M., De Sanctis, M.C., Frigeri, A., LeCorre, L., Preusker, F., Raymond, C.A., Reddy, V., Russell, C.T., Roatsch, T., Schenk, P.M., 2014. Geologic mapping of Vesta. Planet. Space Sci. 103, 2–23. http://dx.doi.org/10.1016/j.pss.2013.12.014i.

Yingst, R.A., Crown, D.A., Mest, S.C., Jaumann, R., Roatsch, T., Preusker, F., Nathues, A., Schaeffer, M., Russell, C.T., Raymond, C.A., 2015. Initial geologic mapping of the AC-H-14 Yalode Quadrangle of Ceres using Dawn spacecraft data. Geol. Soc. Am. Abstracts with Program 47 (7) Abstract 308-14.

Yingst, R.A., Crown, D.A., Sizemore, H.G., Mest, S.C., Berman, D.C., Platz, T., Schmedemann, N., Wagner, R., Preusker, F., Nathues, A., Hoffman, M., Schaefer, M.the Dawn Science Team, 2016. Urvara and Yalode basins: stratigraphic markers in the geologic record of Ceres. Lunar and Planetary Science Conference XLVII, Abstract 1787. Lunar and Planetary Institute.